

Blunt body impact onto viscoelastic floating ice plate with a soft layer on its upper surface

Cite as: Phys. Fluids **33**, 062105 (2021); <https://doi.org/10.1063/5.0047443>

Submitted: 13 February 2021 . Accepted: 10 May 2021 . Published Online: 02 June 2021

 T. I. Khabakhpasheva, and  A. A. Korobkin

COLLECTIONS

 This paper was selected as Featured



View Online



Export Citation



CrossMark

ARTICLES YOU MAY BE INTERESTED IN

[Dynamics of the cavity evolution during vertical water entry of deformable spheres](#)

Phys. Fluids **33**, 065106 (2021); <https://doi.org/10.1063/5.0051401>

[Drag on a spherical particle at the air-liquid interface: Interplay between compressibility, Marangoni flow, and surface viscosities](#)

Phys. Fluids **33**, 062103 (2021); <https://doi.org/10.1063/5.0050936>

[Multiscale modeling of tip-leakage cavitating flows by a combined volume of fluid and discrete bubble model](#)

Phys. Fluids **33**, 062104 (2021); <https://doi.org/10.1063/5.0054795>

Physics of Fluids

SPECIAL TOPIC: Flow and Acoustics of Unmanned Vehicles

Submit Today!



Blunt body impact onto viscoelastic floating ice plate with a soft layer on its upper surface

Cite as: Phys. Fluids **33**, 062105 (2021); doi: [10.1063/5.0047443](https://doi.org/10.1063/5.0047443)

Submitted: 13 February 2021 · Accepted: 10 May 2021 ·

Published Online: 2 June 2021



View Online



Export Citation



CrossMark

T. I. Khabakhpasheva^{a)}  and A. A. Korobkin^{b)} 

AFFILIATIONS

School of Mathematics, University of East Anglia, Norwich NR4 7TJ, United Kingdom

^{a)} Author to whom correspondence should be addressed: t.khabakhpasheva@uea.ac.uk

^{b)} Electronic mail: a.korobkin@uea.ac.uk

ABSTRACT

Two-dimensional vertical impact of a rigid blunt body onto a floating ice plate is studied. The problem is coupled and unsteady. The liquid is inviscid, incompressible, and of infinite depth. The ice floe is modeled as a thin viscoelastic plate of constant thickness. The plate edges are free of bending stresses and shear forces. The upper surface of the plate is covered with a viscoelastic layer of constant small thickness and negligible inertia. The reaction force of this soft layer is predicted by a nonlinear and one-dimensional Winkler-Kelvin-Voigt model, which does not permit a contact between the rigid body and the ice plate. The soft layer may describe either the presence of snow on the ice or a layer of crushed ice in the place of impact, or can be considered as a way of regularization of problems with concentrated loads. The rigid body touches the upper surface of the soft layer and then suddenly starts to move downward with constant velocity. It is shown that the strains in the ice plate caused by the impact are weakly dependent on the characteristics of the soft layer. The magnitudes and distributions of the strains are studied depending on the length of the ice plate, retardation time of the ice model, thickness of the plate, shape of the rigid body, place of impact, and the impact speed. The value of the retardation time in the soft layer model is discussed with relation to the ice crushing by impact.

Published under an exclusive license by AIP Publishing. <https://doi.org/10.1063/5.0047443>

I. INTRODUCTION

The vertical impact by a rigid blunt body onto a floating ice plate is studied within the linear theory of hydroelasticity. The motivation for this study comes from ship navigation and performance of the conventional free fall lifeboats in icy waters. The effect of a single ice floe on slamming loads for sea-going ships and conventional lifeboats is of particular concern, see [Lubbad and Loset \(2011\)](#) and [Re and Veitch \(2003\)](#). [Khabakhpasheva et al. \(2018b\)](#) studied this problem for short ice floes, which were modeled as rigid plates, and symmetric impact conditions. For larger floes, their elastic responses to impacts should be taken into account. Vertical impacts on infinite floating ice plates were studied theoretically and numerically by [Tkacheva \(2007\)](#), [Kozin and Pogorelova \(2006\)](#), [Pogorelova \(2010\)](#), and [Korobkin \(2000\)](#) using the linear theory of potential flows. These authors investigated bending stresses in an elastic floating ice plate caused by an impact on it. [Sodhi \(1989, 1998\)](#) studied the vertical penetration of floating ice plates by an indenter, where the ice fracture plays a major role. The vertical impacts received less attention than the interaction of floating ice plates with vertical walls of offshore structures, see [Nakazawa and Sodhi \(1990\)](#), for example, where the ice fracture and the resulting

forces are of main concern. The problem of horizontal impact on a floating ice sheet is not considered in the present paper.

The problem of impact onto floating elastic plate is similar to the problem of aircraft landing on very large floating platform, see [Watanabe et al. \(1998\)](#), [Kashiwagi \(2004\)](#), and [Qiu \(2007\)](#). However, in the present problem, the impact loads are not given, and they do not move along the plate as a landing aircraft. Impact onto elastic plate, which is placed on water surface, was studied by [Shams et al. \(2017\)](#). The strength of the point impact load was given. The problem was formulated as an integrodifferential equation with respect to the plate deflection and solved by a finite element method.

The vertical impact onto a floating ice floe is studied here as unsteady, linear, two-dimensional, and coupled problem of hydroelasticity. The hydrodynamic loads and elastic ice response are determined at the same time. The ice deflection is described by the equation of viscoelastic Euler plate of constant thickness, see [Brocklehurst et al. \(2011\)](#) and [Shishmarev et al. \(2019\)](#). In contrast to many other studies of ice response to impact on it, we do not assume impact loads but calculate them as part of the solution together with the region of contact between the impacting rigid body and the elastic ice plate. It is known

that such a contact region may consist of several intervals of contact, the positions and lengths of which are determined by the condition that the surface of the rigid body is above the deformed ice plate at any time instant after the impact and the loads acting on the plate are positive. The contact may occur at separate points within some simplified models of elasticity. The problems with concentrated unknown loads and inequalities for elastic deflections and loads are challenging both theoretically and computationally. A practical approach to such problems is to introduce a viscoelastic soft layer between the impacting body and the ice, see [Khabakhpasheva et al. \(2018b\)](#). This layer can model either some physical properties of the ice surface, as in [Khabakhpasheva et al. \(2018b\)](#), the presence of snow on the ice or can be considered as a way of regularization of problems with concentrated loads, or as a penalty method to satisfy the inequality concerning the positions of the body surface and the floating ice plate, see [Kerr \(1964\)](#) and [Younesian et al. \(2019\)](#) for more details.

Practical problems of navigation in ice and vertical impact on ice floes are three-dimensional. However, for an elongated body falling on ice floe with a small heel angle, the floe deflections and stresses in the floe at the middle of the body, where they are maximum, can be approximated as two-dimensional. Such approximation of three-dimensional problems by a sequence of two dimensional ones is well known in ship hydrodynamics as the strip theory, see [Gerritsma and Beukelman \(1967\)](#) and [Loukakis and Scfavounos \(1978\)](#), for elongated ships with small forward speed. Gravity effects and waves radiated by each section of the ship hull are included in ship strip theories. In contrast, local stresses induced by the wave impact on ship hull and/or ship slamming in waves are usually studied both numerically and experimentally within two-dimensional hydroelastic models without account for gravity, viscosity, and surface tension effects, see [Faltinsen et al. \(1997\)](#). These effects can be neglected during the impact stage, which is of short duration with small displacements of impacting bodies. Inertia and dynamic hydroelastic effects play the major role in elastic impact problems and are described using the so-called added-mass matrix for elastic modes of the elastic structure. The experiments confirm that the long-crested wave impact onto elastic plate produces two-dimensional stress distributions in the plate at a short distance from the plate edges. To estimate possible damage to a ship hull caused by slamming, we need a reliable estimate of the maximum local bending stresses, which is provided by the two-dimensional theory. Three-dimensional effects reduce local stresses, see [Faltinsen et al. \(1997\)](#). The problem of a rigid body impact onto a floating elastic plate, which is studied in this paper, is close to the problem of wave impact onto an initially dry and horizontal elastic plate, see [Korobkin and Khabakhpasheva \(2006\)](#), with the following differences. In the problems of wave impact, the wetted part of the plate increases in time, which makes the problem complicated and difficult to study. In our present problem, the elastic plate is in contact with water during the impact stage, and a rigid body impacts the upper surface of the plate.

Motivation for the present study comes, in particular, from the performance and launching a standard free fall lifeboat in ice-covered water. A lifeboat cannot be launched onto continuous ice, but it can be launched in emergency conditions on water covered with some ice floes, if the floes are small enough and not thick. The problems with survival craft in icy water and some experimental campaigns with such craft are described by [Gudmestad and Solberg \(2019\)](#). [Lau et al. \(2006\)](#) write about launching of survival craft on ice-covered waters

“The standard free fall lifeboat in accordance with [IMO \(2016\)](#) provisions includes arrangements that allow only a lowering aft of the ship. It is impossible for a vessel to launch free fall lifeboat onto ice. If a lifeboat should be lowered onto ice, the slope of the bottom of the boat hull must be considered and equipment for limiting the heel must be provided.” For example, totally enclosed lifeboat Viking Norsafe Maggie-10.7 has a length of 10.7 m with a beam of 3.3 m and height of 3.55 m. The estimated mass of the boat with 90 persons inside is 12.7 tons. This lifeboat is elongated and, being lowered without a heel angle onto an ice floe, provides two-dimensional stresses in the floe except near both ends of the craft. To estimate stresses in the floe, this lifeboat can be approximated as a cylinder of radius 1.6 m. The impact speed of the boat on the floe is about 1 m/s if the boat is released 5 cm from the ice surface.

The two-dimensional problem of a body collision with an ice floe is relevant also to the problem of a submarine surfacing from under the ice, see [Conley \(1997\)](#) and [Ye et al. \(2020\)](#), for example. The surfacing problem is different from the problem of this paper because of the hydrodynamic forces between the ice and the approaching submarine. However, the hydrodynamic forces are neglected in [Ye et al. \(2020\)](#). The ice plate is of small constant thickness. The ice is modeled as brittle-plastic material. Numerical and experimental results for three-point bending of columnar ice are compared in Sec. 4.1 of the paper by [Ye et al. \(2020\)](#). The rigid body in these test calculations is not of small curvature as in the present paper. However, the mechanism of the ice failure is the same, as in the present paper, with a crack developed on the opposite surface of the ice plate due to bending of ice and tensile stresses there. Crushing of ice in the place of indentation has not been observed, which can be explained by slow motion of the rigid indenter. The numerical stresses in the ice plate increased almost linearly in time before the ice plate breaking into two pieces in 3 s. Comparison of the numerical stresses and the experimental ones is fairly good. The loads were applied slowly, which suggest that the ice response was quasi-static. In another test problem, with the impact on ice by a circular cylinder, the impact velocity was 0.1 m/s, see Sec. 4.2 in [Ye et al. \(2020\)](#), and the calculations were performed for around 3 s after the start of the ice-body interaction. In models of submarine surfacing, rigid motions of the ice are restricted, the interaction is slow, and hydrodynamic forces can be neglected. The present paper is focused on impact loads with rigid and elastic motions of the ice being of the same order, and hydrodynamic loads playing important role.

Another application of two-dimensional formulations to practical three-dimensional problems in ice-covered waters comes from the performance of high-speed vessels. The corresponding approximate theory known as 2D+T theory is well validated for open water, see [Sun and Faltinsen \(2011\)](#). We unaware of application of this theory to icy waters and level ice. However, we think that 2D+T theory can be useful for the study of dynamic response of high-speed vessels in Arctic navigation as well. Within the 2D+T theory, we introduce a stationary vertical control plane normal to the direction of the vessel motion, if the vessel motion is stationary, and consider the flow and ice response only in this plane within the two-dimensional, unsteady, and non-linear formulation, see [Tassin et al. \(2013\)](#). The two-dimensional flow and ice response in the control plane are equivalent to the problem of a body impact onto the ice sheet, which is studied in the present paper. However, in contrast to the formulation of the present paper, the impacting body within the 2D+T theory changes its

shape in time, see [Tassin et al. \(2013\)](#), which makes the problem more complicated than the present one. To include heave and pitch motions of the vessel, one needs to introduce several 2D vertical planes and formulate equations for dynamic motions of the vessel. [Sun and Faltinsen \(2011\)](#) showed that three-dimensional local corrections should be introduced at the rear part of the vessel to improve the predictions of the vessel motions by the 2D+T theory compared with the experimental results on rough-water performance of planning boats. Application of the 2D+T theory to high-speed vessels in Arctic is challenging because the level ice can be broken by the vessel moving on it. We expect that a combination of the 2D+T theory with the model of impact onto an ice floe with a preexisting crack, see [Korobkin and Khabakhpasheva \(2018\)](#), can provide a consistent theory of navigation in Arctic.

We are unaware of experiments with large rigid body impact onto a floating ice plate, where the ice is broken by bending. Impact and penetration through a floating ice plate of small rigid indentors was studied by many authors, see [Sodhi \(1989, 1998\)](#) and the references therein. For small body impact, the ice crushing and fracture near the impact place play the major role. For large rigid bodies, as studied in the present paper, ice crushing is less important than bending stresses in the ice plate. The present paper is focused on bending stresses in a floating ice plate, which are caused by vertical impact on this plate. The speed of the rigid body during its impact on a floating ice plate is assumed constant, which corresponds to a heavy body such as a lifeboat with 90 persons inside, as mentioned above. The problem of a rigid body impact with a variable in time speed, which should be calculated as a part of the solution together with the impact loads and ice response, can be studied by using the approach of the present paper, see a similar study but for short ice plates, where the elastic plate motions are small, in [Khabakhpasheva et al. \(2018b\)](#). The problem of free-falling body impact is not considered in this paper. Note that three-dimensional effects are more pronounced and important for impacts by small bodies than for impacts by large elongated bodies, which are typical in naval field.

There are many parameters in the impact problem. To limit the number of the parameters, we limit ourselves to parabolic shapes with the only parameter R , which is the radius of the body surface curvature at the point of impact. Only the shape of the part of the body surface, which is in contact with the floating plate, is important for interaction. The shape of the rest of the body does not matter for the stresses in the ice plate caused by impact. We assume that the rigid body does not become wet during the impact. The speed of the body V is constant and equal to 1 m/s in most of the calculations. This corresponds to the case of heavy body impact onto an ice floe. The effect of the impact speed on the strains in ice is studied in Sec. IV B. All calculations here are performed for $R = 5$ m. The maximum strain in the ice plate decreases with increase in R for a constant impact speed V . In the limiting case of a rigid body with flat bottom and of the same length as the ice floe, there are no elastic motions of the plate with zero strains in the plate.

Elastic characteristics of the ice are taken from the available literature. These characteristics depend on temperature and structure of ice. [Schulson \(1999\)](#) reports that Young's modulus of the ice may vary from 9 MPa to 12 GPa, for example. The tensile strength of ice varies from 0.7 to 3.1 MPa, see [Petrovic \(2003\)](#). [Schulson \(1999\)](#) wrote "Brittle behaviour sets in at higher strain rates. Under tension ice

breaks after lengthening 0.01–0.1% through trans-granular cleavage. The tensile strength is rate independent and is only slightly thermally dependent, rising by less than 25% upon decreasing temperature from -5°C to -20°C ." In our notations, it gives the yield strain ϵ_Y in the range from 100 to 1000 microstrains (μstrain). The reference yield strain is taken as $80\ \mu\text{s}$ in the present study. Note that in the case of impulsive loading, the maximum values of elastic strains at a point of the structure or over the structure at a given time instant are not enough to conclude about a crack initiation in the structure and its following failure. [Petrov and Morozov \(1994\)](#) argued that this is an averaged, both in time and space, stress in a structure and should be used as a measure of the structural failure instead of stress at a point and at a certain time instant. They formulated a criterion for fracture, which includes the fracture incubation time and the characteristic size of a fracture process zone. [Bratov and Petrov \(2007\)](#) wrote "The incubation time is constant for a given material and does not depend on problem geometry, the way a load is applied, the shape of a load pulse or its amplitude... the characteristic size of a fracture process zone is constant for the given material and chosen scale." This criterion was successfully applied to explain some experimental data. It was included in a peridynamic model of dynamic crack initiation, see [Ignatev et al. \(2020\)](#). This criterion of structural fracture implies that the ice plate impacted by a rigid body can survive even the strain at a single point and at a certain time instant achieves the yield value. The incubation time is of order of several microseconds. For example, it is equal to $44\ \mu\text{s}$ for gabbro-diabase, see [Peck \(2018\)](#). The process of a crack initiation and/or crack growth caused by impact loads is more complicated and requires a special analysis. This explains why we do not terminate our calculations when the local strain approaches the selected yield value. The problems of a crack initiation and crack growth are not considered in this paper. The model developed in this paper is robust and quick in producing reliable results. It can be used for preliminary estimates of floating ice response to vertical impact on it.

In contrast to some investigations of ice response, where the hydrodynamic effects are neglected, see [Ye et al. \(2020\)](#), we study here only the cases, where a floating elastic plate response strongly depends on hydrodynamic loads. We study problems of hydroelasticity, where the flow is caused by elastic plate motions, and the elastic plate motions are affected by the hydrodynamic loads. The problems of hydroelasticity are coupled. The flow, hydrodynamic pressure, and the plate response should be determined at the same time. Initially, the floating plate and the liquid are at rest. Then, the plate is suddenly accelerated by an impacting body. The initial interaction stage, when the plate is accelerated, starts to vibrate, and then separates from the impacting body, is of short duration. Gravity, surface tension, and viscous effects are negligible during this short stage compared with inertia of the plate and liquid. The flow is potential, see [Korobkin and Pukhnachov \(1988\)](#). The displacements of both the plate and the liquid are small, which make it possible to linearize the equations of motion and the boundary conditions and impose the linearized boundary conditions at the initial position of the flow boundary. The resulting linearized problem has periodic in time solutions if the structural damping is neglected. There is no hydrodynamic damping in this formulation because both the gravity and liquid viscosity are neglected in the leading order. The lowest period T_1 of such solutions, which are known as wet modes, depends on the plate length, plate rigidity, and the liquid density. The plate response to the impact strongly depends

on the hydrodynamic loads if the duration of impact is close to T_1 , see [Faltinsen et al. \(2004\)](#). If the impact loads are applied during the initial stage, which is longer than T_1 , then the hydrodynamic loads are less important and can be treated as quasi-static ones, as it was done by [Ye et al. \(2020\)](#). In this paper, we consider impact conditions and the characteristics of the floating plate, see Sec. IV A, such that the duration of the impact stage is close to T_1 and the plate response is strongly affected by the hydrodynamic loads. The problems, where the hydrodynamic and structural parts are strongly coupled, are still difficult to solve numerically, see [Korobkin and Malenica \(2016\)](#), because a hydrodynamic CFD solver and a structural FEM solver need an interface, allowing them to solve the hydrodynamic and structural problems at the same time.

Detailed analysis of the ice response requires a finite-element model (FEM) of ice with an account for its type, temperature, salinity and other characteristics of a particular ice, and a computational fluid dynamic (CFD) model of hydrodynamic forces during the impact on floating ice. An FEM of ice should include models of ice fracture with a crushing and an initiation of cracks, and a model of ice porosity, see [Ye et al. \(2020\)](#). Such a CFD+FEM model contains many parameters, values of which are different for different ice types and different impact conditions. Dedicated experiments are needed to fit the parameters to the experimental results, see [Sebastiro \(2013\)](#), who treats a model fitting as an art. Blind tests should be performed to justify the model and the values of the parameters. This is a time-consuming procedure, which should be done again for another ice in another place. These difficulties with modeling of everything in full details explain the need for parsimonious models, which explain and reasonably predict physical processes with a minimum number of parameters. The principle of parsimony implies that research should search for simple measurement and theoretical models that use the minimum number of parameters needed to explain a given phenomenon, see [Raykov and Marcoulides \(1999\)](#). A parsimonious model explains a phenomenon and identifies the most interesting cases, but the numerical results should be computed by more detailed models.

II. FORMULATION OF THE PROBLEM

The two-dimensional unsteady problem of a rigid body impact onto a floating viscoelastic ice plate covered with a thin viscoelastic layer of another material, which is called below a soft layer, is studied. The plate of a length $2L$ and a thickness h_i is floating on the liquid surface. Initially, the liquid is at rest and occupies a lower half-plane, $y < 0$. In the Cartesian coordinate system xOy , see [Fig. 1](#), the interval $y = -d, -L < x < L$ corresponds to the lower flat surface of the plate, where d is the draft of the plate, $d = h_i(\rho_i/\rho)$, ρ_i is the ice density, and ρ is the liquid density. The upper surface of the ice plate is at

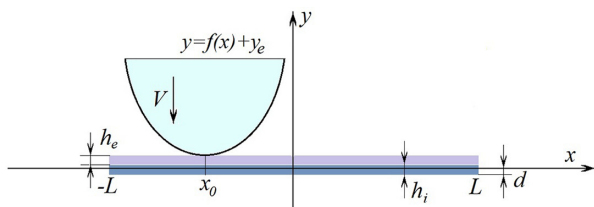


FIG. 1. Initial positions of the floating ice plate and the rigid body.

the level $y = -d + h_i$. The ice plate is thin, $h_i/L \ll 1$, in this study. The soft layer on the top of the ice plate is of constant thickness h_e . A rigid body touches the upper surface of the soft layer at a single point, $y = y_e$ and $x = x_0$, where $-L < x_0 < L$ and $y_e = h_e + h_i - d$. The position of the body surface at a time t is described by the equation, $y = y_e + f(x) - Vt$, where $f(x_0) = 0$ and $f(x) > 0$ for $x \neq x_0$. The shape function $f(x)$ is taken parabolic in this study, $f(x) = (x - x_0)^2/(2R)$, where R being the radius of curvature of the parabola.

At some instant of time, taken as initial one, $t = 0$, the body suddenly starts to move downward with a constant speed V pushing the soft layer and the ice plate into the liquid. The liquid is assumed ideal and incompressible. The flow generated by the impact is assumed two-dimensional and potential. During the early impact stage, both the equations of the ice plate deflection and the equations of the flow can be linearized. The boundary conditions of the hydrodynamic part of the problem can also be approximately linearized and imposed on the initial liquid level, $y = 0$. The flow caused by an impact is inertia dominated with gravity, viscous effects, and surface tension playing minor roles because of short duration of the impact stage, see [Greenhow \(1987\)](#) and [Khabakhpasheva and Korobkin \(2013\)](#) for justification of this approximation.

These assumptions lead us to a linearized unsteady problem of hydroelasticity. However, the relation between the impact load and the ice plate deflection is non-linear. We shall determine the deflection of the viscoelastic ice plate, the stresses in the plate, and the impact loads acting on the plate together with the corresponding intervals, where the loads are applied, during the early stage of impact when the ice deflection and the rigid body displacement are small.

The position of the ice/liquid interface is described by the equation $y = -d + w(x, t)$, where $w(x, t)$ is the deflection of the ice plate, see [Fig. 2](#). The vertical displacement of the rigid body is shown as $s(t)$ in [Fig. 2](#), where $s(0) = 0$ and $s'(0) = V$. For constant velocity of impact, we have $s(t) = Vt$. The ice deflection is governed by the following equation of thin viscoelastic plate, see [Squire et al. \(1996\)](#):

$$m \frac{\partial^2 w}{\partial t^2} + EJ \left(1 + \tau_i \frac{\partial}{\partial t} \right) \frac{\partial^4 w}{\partial x^4} = p(x, t) - \left(1 + \tau_e \frac{\partial}{\partial t} \right) P_e(x, t) \quad (|x| < L, t > 0), \tag{1}$$

where E is the Young's modulus of the ice, $J = h_i^3/12$ is the moment of inertia of the ice plate cross section, $m = h_i \rho_i$ is the mass of the ice plate per unit area, and $p(x, t)$ is the hydrodynamic pressure acting on the ice/liquid interface. The edges of the plate are free of bending stresses and the shear force,

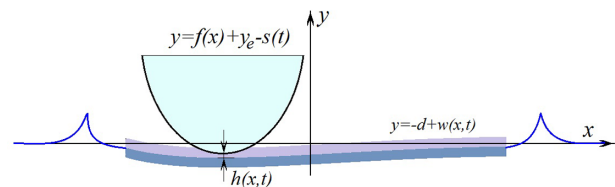


FIG. 2. Deflection of the ice plate and compression of the soft layer on the top of the ice plate by the impacting body.

$$\frac{\partial^2 w}{\partial x^2}(\pm L, t) = 0, \quad \frac{\partial^3 w}{\partial x^3}(\pm L, t) = 0. \tag{2}$$

Initially, the ice plate is at rest,

$$w(x, 0) = 0, \quad \frac{\partial w}{\partial t}(x, 0) = 0 \quad (|x| < L). \tag{3}$$

The reaction force, $(1 + \tau_e \partial/\partial t)P_e(x, t)$, of the soft layer to the rigid body impact is assumed to be given by a nonlinear one-dimensional Winkler-Kelvin-Voigt model and depends on the current local thickness of the layer and its time derivative, where τ_e is the retardation time responsible for the energy dissipation in the soft layer. Here, $P_e(x, t) = KG(\delta)$, where $\delta(x, t)$ is the relative compression of the layer if $\delta > 0$, K is the rigidity of the material of the soft layer, and the function $G(\delta)$ is such that $G(\delta) = 0$ for $\delta \leq 0$, which is in places without contact between the rigid surface and the soft layer, $G(\delta) \sim \delta$ for small positive δ , which corresponds to Hooke’s law, and $G(\delta) \rightarrow \infty$ as $\delta \rightarrow 1$, which is where the rigid surface approaches the surface of the ice plate. This function is taken in the form $G(\delta) = \delta/(1 - \delta)$, where

$$\delta(x, t) = \frac{h_e - h(x, t)}{h_e}, \quad h(x, t) = f(x) - Vt - w(x, t) + h_e, \tag{4}$$

where $h(x, t)$ is the vertical distance between the ice upper surface and the rigid surface of the body. The intervals of contact between the surface of the rigid impacting body and the soft layer are defined by the inequality $h(x, t) < h_e$. The relative compression of the soft layer, $\delta(x, t)$, is not small in the present model.

The hydrodynamic pressure, $p(x, t)$, in the plate equation (1) is given by the linearized Bernoulli equation without account for the hydrostatic pressure,

$$p(x, t) = -\rho\varphi_t(x, 0, t), \tag{5}$$

where the velocity potential $\varphi(x, y, t)$ is the solution of the following boundary-value problem:

$$\begin{aligned} \nabla^2 \varphi &= 0 \quad (y < 0), \quad \frac{\partial \varphi}{\partial y} = \frac{\partial w}{\partial t} \quad (|x| < L, y = 0), \\ \varphi &= 0 \quad (|x| > L, y = 0), \quad \varphi \rightarrow 0 \quad (x^2 + y^2 \rightarrow \infty). \end{aligned} \tag{6}$$

The flow under the plate is caused by both rigid and elastic motions of the impacted plate, which are small during the impact stage of short duration. The deflections of the floating plate are small compared with the plate length. This makes it possible to linearize the equations of the flow together with the boundary conditions, and impose the boundary conditions at the initial liquid level, $y=0$, see Korobkin and Pukhnachov (1988). The linearized dynamic, which the hydrodynamic pressure at the free surface is equal to the atmospheric pressure, and the kinematic, which the liquid particles on the free surface move together with this surface, free-surface conditions provide $\varphi(x, 0, t) = 0$ and $(\partial\varphi/\partial y)(x, 0, t) = (\partial\eta/\partial t)(x, t)$, where $|x| > L$, see equation (5). The equation $y = \eta(x, t)$ describes the elevation of the free surface caused by the impact. The velocity potential $\varphi(x, y, t)$ satisfies the Laplace’s equation in the linearized flow domain, $y < 0$, the linearized body boundary condition at the linearized position of the plate lower surface, $|x| < L, y = 0$, and decays at infinity far from the plate. Note that the kinematic boundary condition on the free surface is not included in the hydrodynamic problem (6). This condition is needed if

the wetted part of the plate changes in time, see Korobkin and Pukhnachov (1988). However, in the present problem of impact onto a floating plate, the wetted part of the plate does not change in time. Therefore, the kinematic condition $(\partial\varphi/\partial y)(x, 0, t) = (\partial\eta/\partial t)(x, t)$, where $(|x| < L, y = 0)$, is considered here as the equation for the free-surface elevation, where the derivative $(\partial\varphi/\partial y)(x, 0, t)$ is obtained from the hydrodynamic problem (6) and initially $\eta(x, 0) = 0$. Note that the fact that the boundary conditions are imposed on the initial level of the liquid does not mean that the free surface is stay at $y = 0$ during the impact. The shape of the free surface is calculated by integrating the kinematic condition in time. Moreover, within the linearized hydrodynamic model (6), the vertical velocity of the free surface at the plate edges is square-root singular. As a result, the elevation of the free surface at the plate edges behaves as $\eta(x, t) = O([x^2 - L^2]^{-1/2})$ as $|x| \rightarrow L + 0$. Such shape of the free surface is not physical and has been corrected through the local asymptotic and numerical analysis of the flow close to the plate edges, see Iafrazi and Korobkin (2004, 2008). These arguments explain a particular shape of the free surface sketched in Fig. 2, see also Fig. 6 from Iafrazi and Korobkin (2004).

Note that the hydrostatic pressure, $-\rho gw(x, t)$, is neglected in the Bernoulli equation (5) compared with the dynamic component of the pressure. The ratio of these two components, $\rho\varphi_t/(\rho gw)$, where $\varphi = O(wL/T)$ from (6) and T is the duration of the impact stage, is of the order $O(gT^2/L)$, which is small for short duration of the impact stage and long plates, see conditions of numerical calculations in Sec. IV.

The formulated problem (1)–(6) is coupled. The ice deflection, $w(x, t)$, and the strains in the ice plate depend on the hydrodynamic pressure, see equation (1), which, in turn, depends on the ice deflection through the kinematic boundary condition in (6) on the surface of the ice plate. The present formulation assumes that the lower surface of the ice plate is in contact with the liquid at any time during the impact stage. This implies that the edges of the floating plate are not allowed to exit from the liquid, and both possible cavitation and ventilation caused by the ice plate vibration are not included in the model. This assumption can be validated *a posteriori* by analyzing the hydrodynamic pressure $p(x, t)$ along the plate, $-L < x < L$.

Dimensionless variables are used below. They are denoted by the same symbols as the corresponding dimensional variables but with tilde. The half-length of the ice plate L is taken as the length scale, $x = L\tilde{x}$ and $y = L\tilde{y}$. The thickness h_e of the soft layer is taken as the displacement and deflection scale, $w = h_e\tilde{w}(\tilde{x}, \tilde{t})$ and $t = \tilde{t}h_e/V$. The displacement scale was chosen to accurately resolve in time the compression of the soft layer and correspondingly the loads acting on the ice plate. This is, the plate deflection can be much greater than h_e but it should be much smaller than L . The scale of the velocity potential $L\tilde{V}$ follows from the kinematic condition on the ice/liquid interface. Then, the scale of the hydrodynamic pressure is $\rho V^2 L/h_e$. The strains $\varepsilon(x, t)$ are of particular concern in the impact problem of hydroelasticity. In the dimensionless variables, $\varepsilon(\tilde{x}, \tilde{t}) = \varepsilon_{sc}\tilde{w}_{\tilde{x}\tilde{x}}(\tilde{x}, \tilde{t})$ on the lower surface of the ice plate with the strain scale $\varepsilon_{sc} = h_e h_e/(2L^2)$. Positive value of the strain implies that this part of the lower surface of the ice is in tension. This may lead to ice cracking in this place if the strain is greater than the so-called yield strain ε_Y , see Brocklehurst *et al.* (2011), where $\varepsilon_Y = 8 \times 10^{-5}$.

In the dimensionless variables (tilde is dropped below), the plate equation (1), the edge (2), and initial (3) conditions read

$$\alpha_1 \frac{\partial^2 w}{\partial t^2} + \beta \left(1 + \tilde{\tau}_i \frac{\partial}{\partial t} \right) \frac{\partial^4 w}{\partial x^4} = -\alpha \frac{\partial \varphi}{\partial t} - \left(1 + \tilde{\tau}_e \frac{\partial}{\partial t} \right) G(\delta) \quad (7)$$

(|x| < 1, t > 0),

$$\frac{\partial^2 w}{\partial x^2}(\pm 1, t) = 0, \quad \frac{\partial^3 w}{\partial x^3}(\pm 1, t) = 0, \quad (8)$$

$$w(x, 0) = 0, \quad \frac{\partial w}{\partial t}(x, 0) = 0 \quad (|x| < 1), \quad (9)$$

where

$$\delta(x, t) = w(x, t) + t - \hat{d}(x - \epsilon)^2, \quad (10)$$

$$G(\delta) = \frac{\delta}{1 - \delta} \quad (0 < \delta < 1), \quad G(\delta) = 0 \quad (\delta < 0).$$

The velocity potential $\varphi(x, y, t)$ is the solution of the following boundary-value problem,

$$\nabla^2 \varphi = 0 \quad (y < 0), \quad \frac{\partial \varphi}{\partial y} = \frac{\partial w}{\partial t} \quad (|x| < 1, y = 0), \quad (11)$$

$$\varphi = 0 \quad (|x| > 1, y = 0), \quad \varphi \rightarrow 0 \quad (x^2 + y^2 \rightarrow \infty).$$

There are seven dimensionless parameters in the formulated problem,

$$\alpha_1 = \frac{\rho_i h_i V^2}{K h_e}, \quad \beta = \frac{E J h_e}{L^4 K}, \quad \alpha = \frac{\rho L V^2}{K h_e}, \quad (12)$$

$$\tilde{\tau}_i = \frac{\tau_i V}{h_e}, \quad \tilde{\tau}_e = \frac{\tau_e V}{h_e}, \quad \hat{d} = \frac{L^2}{2 R h_e}, \quad \epsilon = \frac{x_0}{L},$$

all of them are in the plate equation (7) and in the definition of the relative compression of the soft layer, $\delta(x, t)$, see (10).

III. NORMAL MODE METHOD

The formulated problems (7)–(11) of vertical impact on a floating ice floe are solved by the normal mode method (Kvalsvoild, 1994; Korobkin, 1998; Korobkin and Khabakhpasheva, 1998; Korobkin and Khabakhpasheva, 2006). The ice deflection is sought in the form

$$w(x, t) = \sum_{n=1}^{\infty} a_n(t) \psi_n(x), \quad (13)$$

where $\psi_n(x)$ are the so-called normal modes of the dry elastic plate and $a_n(t)$ are the principal coordinates of the modes, which are to be determined. The normal modes are non-zero solutions of the eigenvalue problem,

$$\frac{d^4 \psi_n}{dx^4} = \lambda_n^4 \psi_n \quad (-1 < x < 1), \quad (14)$$

$$\frac{d^2 \psi_n}{dx^2} = 0, \quad \frac{d^3 \psi_n}{dx^3} = 0 \quad (x = \pm 1),$$

where λ_n is a spectral parameter, $n \geq 1$. There are two modes, $n = 1$ and $n = 2$, with $\lambda_1 = \lambda_2 = 0$, which correspond to rigid motions of the plate,

$$\psi_1(x) = \frac{1}{\sqrt{2}}, \quad \psi_2(x) = \sqrt{\frac{3}{2}} x. \quad (15)$$

The modes starting from $n = 3$ correspond to elastic deflections of the plate,

$$\psi_n(x) = A_n \cos(\lambda_n x) + B_n \sin(\lambda_n x) + C_n e^{-\lambda_n(1+x)} + D_n e^{-\lambda_n(1-x)}, \quad (16)$$

where λ_n is a real positive root of the equation

$$\cosh(2\lambda_n) \cos(2\lambda_n) = 1 \quad (17)$$

and the coefficients A_n, B_n, C_n and D_n in (16) are

$$A_n = \frac{1}{\sqrt{2} \cos \lambda_n}, \quad B_n = 0, \quad C_n = \frac{1}{\sqrt{2}(1 + e^{-2\lambda_n})},$$

$$D_n = C_n, \quad n = 2m + 1, \quad A_n = 0, \quad B_n = \frac{1}{\sqrt{2} \sin \lambda_n}, \quad (18)$$

$$C_n = \frac{-1}{\sqrt{2}(1 - e^{-2\lambda_n})}, \quad D_n = -C_n, \quad n = 2m + 2.$$

The modes (15) and (16) are orthonormal,

$$\int_{-1}^1 \psi_n(x) \psi_m(x) dx = \delta_{nm}, \quad (19)$$

where $\delta_{mm} = 1$ and $\delta_{nm} = 0$ for $n \neq m$, and $n, m \geq 1$. For large n , we find

$$\lambda_n = \frac{\pi}{4}(n - 2) + O(e^{-\frac{\pi}{2}n}), \quad |C_n| = \frac{1}{\sqrt{2}} + O(e^{-\frac{\pi}{2}n}).$$

The series (13) and the hydrodynamic problem (11) suggest the following series for the velocity potential:

$$\varphi(x, y, t) = \sum_{n=1}^{\infty} \dot{a}_n(t) \varphi_n(x, y), \quad (20)$$

where the overdot stands for time derivative, $\dot{a}(t) = da/dt$, and $\varphi_n(x, y)$ are the solution of (11) with $\partial \varphi_n / \partial y(x, 0) = \psi_n(x)$ in the interval $-1 < x < 1$. The potentials $\varphi_n(x, y)$ do not depend on the motions of the ice plate.

Substituting (13) and (20) in (7), and using (14), (19), and (9), we obtain the following system of ordinary differential equations for the coefficients $a_n(t)$:

$$\frac{d\vec{a}}{dt} = -(\alpha_1 I + \alpha S)^{-1} [\vec{u} + \tilde{\tau}_i \beta D \vec{a} + \tilde{\tau}_e \vec{P}], \quad (21)$$

$$\frac{d\vec{u}}{dt} = \beta D \vec{a} + \vec{P}, \quad \vec{a}(0) = 0, \quad \vec{u}(0) = 0.$$

Here, $\vec{a} = (a_1, a_2, a_3, \dots)^T$ is the vector of unknown coefficients in (13), I is the unit matrix, D is the diagonal matrix, $D = \text{diag}(\lambda_1^4, \lambda_2^4, \lambda_3^4, \dots)$, note that $\lambda_1 = \lambda_2 = 0$, and S is the added-mass matrix with the elements S_{nk} ,

$$S_{nk} = \int_{-1}^1 \varphi_k(x, 0) \psi_n(x) dx, \quad (22)$$

and the elements of the vector $\vec{P}(t, \vec{a}) = (P_1(t, \vec{a}), P_2(t, \vec{a}), P_3(t, \vec{a}), \dots)^T$ are given by the integrals

$$P_n(t, \vec{a}) = \int_{-1}^1 G(\delta(x, t)) \psi_n(x) dx, \quad (23)$$

with the relative compression $\delta(x, t)$ given by (10). The auxiliary vector $\vec{u} = (u_1(t), u_2(t), u_3(t), \dots)^T$ is needed to calculate the time derivatives $\dot{a}_n(t)$.

The integrals (23) are evaluated numerically at each time step of the integration of system (21). The interval $-1 < x < 1$ is derived in N_i subintervals $x_j < x < x_{j+1}$, where $x_j = -1 + (j - 1)\Delta x$, $\Delta x = 2/N_i$, $1 \leq j \leq N_i + 1$. For given vector \vec{a} and time t , we calculate $w(x_j, t)$ by (13) and $\delta(x_j, t)$ by (10). Only subintervals, where $\delta(x, t) > 0$, matter. In such subintervals, $G(\delta(x, t))$ is linearly approximated, and the integrals for each such subintervals are evaluated analytically. In this way, we calculate the integrals (23) accurately even for large n .

In the dimensionless variables, the impact pressure, $\tilde{P}_i(x, t)$, acting on the ice plate through the soft layer is calculated by

$$\begin{aligned} \tilde{P}_i(x, t) &= \left(1 + \tilde{\tau}_e \frac{\partial}{\partial t}\right) \tilde{P}_e(x, t), \quad \delta = w(x, t) + t - \hat{d}(x - \epsilon)^2, \\ \tilde{P}_e(x, t) &= \frac{\delta}{1 - \delta} \quad (0 < \delta < 1), \quad \tilde{P}_e(x, t) = 0 \quad (\delta < 0) \end{aligned} \tag{24}$$

with its scale being equal to the rigidity coefficient of the soft layer K . Note that

$$\begin{aligned} \tilde{P}_i(x, t) &= \frac{\delta}{1 - \delta} + \frac{\tilde{\tau}_e}{(1 - \delta)^2} \left(1 + \frac{\partial w}{\partial t}\right) \quad (0 < \delta < 1), \\ \tilde{P}_i(x, t) &= 0 \quad (\delta < 0) \end{aligned}$$

is not equal to zero at the initial contact point, $x = \epsilon$, at $t = 0$, where $\tilde{P}_e(\epsilon, 0) = 0$ and $\tilde{P}_i(\epsilon, 0) = \tilde{\tau}_e$ because of the viscous properties of the soft layer. Therefore, dissipative properties in the soft layer are expected to make both the impact load and ice plate response smooth in time but not just after the impact instant, when these properties increase the loads. Initially, the interval, where the impact load is applied, starts from a single point $x = \epsilon$. Special treatment of the problem is needed for this early stage because the interval of loading quickly increases in time.

The matrix S is symmetric, $S_{nk} = S_{kn}$, where $n \geq 1$ and $k \geq 1$. The elements of this matrix are given by analytical formulas through λ_n , the coefficients in (18), and Bessel functions, $J_0(\lambda_n)$, $J_1(\lambda_n)$, $I_0(\lambda_n)$, $I_1(\lambda_n)$. These formulas are not given in this paper. The nonlinear system of ordinary differential equations (21) is truncated and integrated in time by the fourth-order Runge-Kutta method.

IV. NUMERICAL RESULTS

Calculations are performed for ice plates with the Young modulus $E = 4.2 \times 10^9$ Pa and density $\rho_i = 917$ kg/m³. Density of water is $\rho = 1000$ kg/m³. The impacting rigid body is parabolic with a radius of curvature $R = 5$ m. The thickness of the soft layer is $h_e = 1$ cm. Elastic characteristics of the ice plate, shape of the rigid body, and the thickness of the soft layer do not vary in the present calculations. We focus our study on dependence of the ice plate response on viscous properties of both the ice and the soft layer, length and thickness of the plate, place of impact, and impact speed. The effects of the body shape and the soft layer thickness on viscoelastic plate response require additional study. Larger radius R of the body curvature and larger thickness of the soft layer are expected to increase the region, where the impact loads are applied to the plate, which lead to a decrease in the plate deflections and, as a result, to a decrease in strains in the plate.

TABLE I. Parameters of calculations.

	K (MPa)	τ_e (s)	τ_i (s)
Case 1	1	0	0
Case 2	1	0.1	0
Case 3	1	0	0.01
Case 4	1	0.1	0.01
Case 5	0.02	0.1	0.01

A. Viscous effects on impact loads and strains

To investigate the effects of both the rigidity coefficient of the soft layer, K , and the retardation times of the soft layer, τ_e , and of the ice plate, τ_i , on the impact loads and strains in the ice plate, five cases are considered, see Table I. In these calculations, the velocity of impact is $V = 1$ m/s, thickness of the ice plate is $h_i = 15$ cm, and the half-length of the plate is $L = 2.5$ m.

The system (21) is truncated to $2N_{mod}$ equations of first order, where N_{mod} is the number of terms retained in the series (13) for the ice plate deflection. The number N_{mod} is determined for each case from Table I separately by investigating the convergence of the strains $\epsilon(x, t)$ as the number increases. The strains are more sensitive to the number of retained terms than the deflection (13). For all cases from Table I, $N_{mod} = 20$ was found to provide accurate solutions, see Table II and Fig. 10 at the end of this subsection. All calculations are performed up to the dimensional time 0.25 s, which corresponds to the maximum displacement of the body 25 cm. Then, the ice plate deflections are smaller than 0.25 m, which is 1/10 of the half-length of the plate. The linear theory of hydroelasticity and the model of thin viscoelastic ice plate are justified for such small deflections.

The system (21) is integrated in the dimensionless variables. For example, the values of the dimensionless parameters (12) for case 4 from Table I and impact at the center of the plate, $x_0 = 0$, are

$$\begin{aligned} \alpha_1 &= 0.013755, \quad \beta = 0.0003024, \quad \alpha = 0.25, \\ \tilde{\tau}_i &= 1, \quad \tilde{\tau}_e = 10, \quad \hat{d} = 62.5, \quad \epsilon = 0. \end{aligned}$$

For case 5, the parameters α , α_1 , and β are five times greater than those shown above. The dimensionless time step is selected as 10^{-4} for case

TABLE II. Maxima of the normal mode coefficients, $\max|a_n(t)|$, during the impact stage, $0 < t < 0.25$ s, calculated for Cases 1, 2, and 4.

n	Case 1 a_n	Case 2 a_n	Case 4 a_n
3	5.96522	6.00713	4.27796
5	0.81520	0.53939	0.23748
7	0.12792	0.12802	0.03944
9	0.03016	0.03574	0.00997
11	0.00969	0.01549	0.00404
13	0.00399	0.00688	0.00175
15	0.00173	0.00354	0.00092
17	0.00086	0.00217	0.00050
19	0.00045	0.00123	0.00030

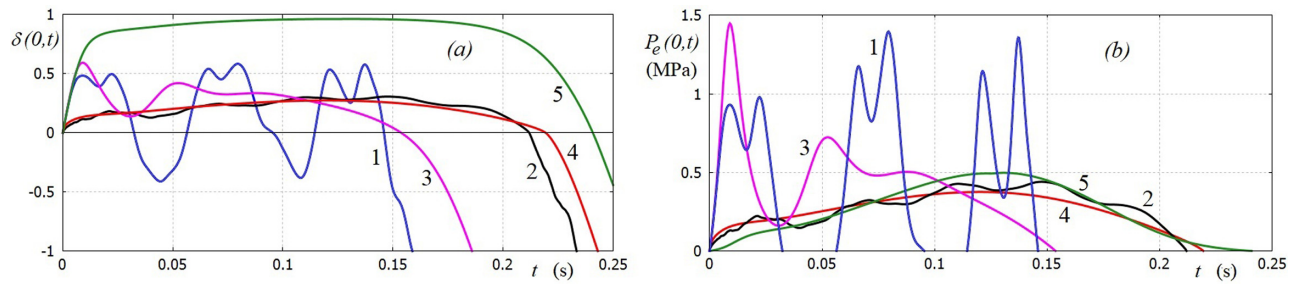


FIG. 3. The relative compression of the soft layer (a), and dimensional pressure (b) at $x=0$ as functions of the dimensional time t for the cases 1–5. Line numbers correspond to the case numbers from Table I. The soft layer is compressed there, where $0 < \delta(0, t) < 1$.

1, which is without dissipation both in the ice and in the soft layer, and 5×10^{-4} for all other cases. The time step depends on accurate resolution of the impact loads and the relative compression $\delta(x, t)$. If the time step is too large, then the computed compression $\delta(x, t)$ could be greater than 1 at a subsequent time step, which is not allowed in the present model. The strains are calculated by the formula

$$\varepsilon(x, t) = \varepsilon_{sc} \sum_{n=3}^{N_{mod}} a_n(t) \psi_n''(x), \quad \varepsilon_{sc} = \frac{h_e h_i}{2L^2}, \quad (25)$$

where $\varepsilon_{sc} = 120$ microstrains (μ strain) for the present impact conditions, 1μ strain $= 10^{-6}$. Note that the scale of the elastic strains and calculated strains, see below, can be greater than the yield strain ε_Y of the ice. Formally, for the present impact conditions, the ice plate is predicted to be broken at the very early stage of the impact with a crack formed at the lower surface of the plate. The growth of the crack and its effect on the strains in the plate are not covered in the present study, see Korobkin and Khabakhpasheva (2018) for a model of a crack development by impact onto a floating plate.

The relative compressions of the soft layer, $\delta(0, t)$, at the impact point, $x=0$, for the cases from Table I are shown in Fig. 3(a) as functions of the dimensional time. Note that $h_e = 1$ cm in the present calculations. Therefore, the vertical axis in Fig. 3(a) can be considered as the depth of penetration of the impacting body into the soft layer measured in centimeters. Negative values of $\delta(0, t)$ mean that the rigid body is above the soft layer at the distance $-\delta h_e$ from its upper surface.

Velocity of the rigid body is 1 m/s. Time $t = 0.1$ s corresponds to the body displacement 10 cm. Without account for viscous effects in both the ice plate and the soft layer, see Fig. 3(a) case 1, the ice plate bounces from the moving body surface three times. The ice plate bounces twice because of elasticity of the soft layer, and the third time at $t \approx 0.15$ s because of elastic vibration of the plate. It is possible that the body touches the soft layer again after $t = 0.25$ s, but then the ice plate displacement will be greater than $0.1L$, and the linearization of the hydrodynamic problem is not justified. Lines 2, 3, and 4 in Fig. 3(a) demonstrate the importance of dissipation in both the soft layer and ice plate for the interaction of the ice plate with the moving body. The lines 2 and 4 are close to each other, which indicates that the dissipation in the soft layer is more important for the impact loads than viscous properties of the ice. The impact energy is well dissipated in cases 2–4, but finally, the ice plate still separates from the body surface due to the elastic vibration of the plate. For the reduced rigidity coefficient, $K = 0.02$ MPa in case 5, the soft layer is compressed almost

completely with δ being close to 1, but finally, the ice plate still separates from the body surface. However, the separation occurs later than for other cases.

To study the effect of the retardation times on the dimensional impact loads, they are decomposed as, see dimensionless equation (24),

$$P_i = P_e(x, t) + P_\tau(x, t), \quad P_e(x, t) = KG(\delta), \quad P_\tau(x, t) = \tau_e \frac{\partial P_e(x, t)}{\partial t}.$$

For the cases 1 and 3, where $\tau_e = 0$, we have $P_i(x, t) = P_e(x, t)$. Evolutions of the elastic part of the impact loads, $P_e(0, t)$, at the impact point for all five cases are shown in Fig. 3(b). It is seen that this component strongly depends on the retardation time of the soft layer. The curves 2, 4, and 5, which correspond to $\tau_e = 0.1$ s but different for τ_i and K , are close to each other and very different from the curves 1 and 3, which are for $\tau_e = 0$.

Distributions of the impact loads, $P_i(x, t)$, along the part of the ice plate, which is in contact with impacting body, are shown in Fig. 4 for cases 1 and 3. The soft layer is pure elastic without account for viscous effects in these cases.

In case 1, see Fig. 4(a), the rigid parabolic body is in contact with the soft layer three times during the initial 0.15 s. The length of the contact region does not exceed 70 cm for the 5 m long plate and the radius of the body curvature 5 m. Figure 3(a) shows that $\delta(0, t) < 0.6$ for case 1, which provides the maximum contact interval $|x| < 24$ cm without account for the plate bending. The actual contact interval is longer than this prediction, which is related to the deflection of the ice plate caused by the impact.

The viscoelastic plate, see Fig. 4(b) for case 3, does not separate from the impacting body during the initial 0.15 s, but the loads are smaller than in case 1, except the very initial stage, see also Fig. 3(b). The contact interval is within $|x| < 24$ cm, which indicates that the deflections of the plate in case 3 are much smaller than in case 1. One may conclude that viscous properties of the ice plate reduce the plate deflections making the plate behave as a more rigid one.

Viscous properties of the soft layer affect the impact loads. The evolutions of the impact pressure, $P_i(0, t)$ by blue lines, together with its elastic, $P_e(0, t)$ by black lines, and viscous, $P_\tau(0, t)$ by red lines, components at the point of initial impact $x=0$ are shown in Fig. 5 for cases 2, 4, and 5 with $\tau_e = 0.1$ s and different τ_i and K . Note that $P_e(0, 0) = 0$ in all cases but $P_\tau(0, 0) = \tau_e KV/h_e$, which gives $P_i(0, 0) = 10$ MPa in cases 2 and 4, and $P_i(0, 0) = 0.2$ MPa in case 5, see Fig. 5.

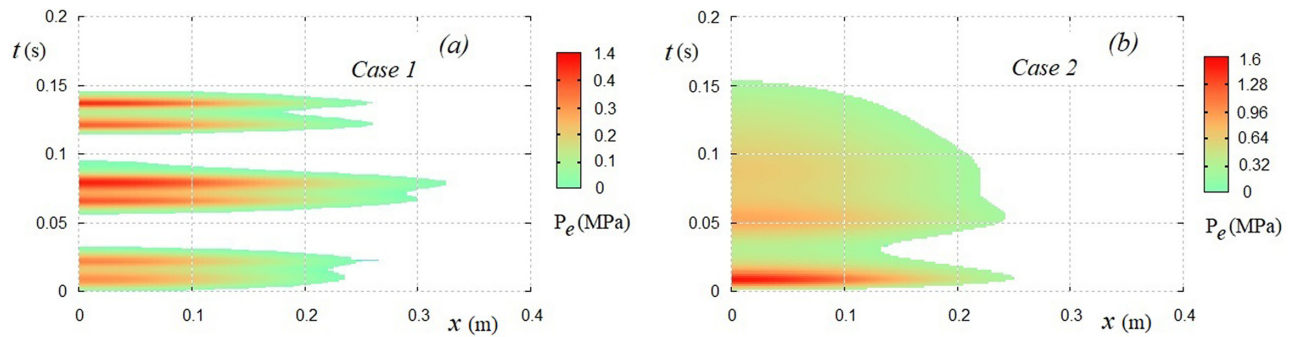


FIG. 4. Distributions of impact loads $P_i(x, t)$ for cases 1 (a) and 3 (b).

The elastic component, $P_e(0, t)$, is smooth and positive in all cases, but the viscous component, $P_\tau(0, t)$, is negative at the end of the impact, see Figs. 5(a)–5(d), and oscillating at the beginning of impact if $\tau_i = 0$, see Fig. 5(a). This leads to tensile impact loads at the end of impact stage and high loads at the beginning of impact within a model of viscoelastic soft layer. To confirm the accuracy of calculated impact loads in case 2, they were computed with different number of retained modes, see Fig. 5(b).

Distributions of the impact loads, $P_i(x, t)$, and their elastic components, $P_e(x, t)$, in time and along the ice plate are shown in Fig. 6 for cases 2, 4, and 5 with $\tau_e = 0.1$ s. Figure 6 confirms the conclusions drawn on the basis of Fig. 5 that the viscous properties of the soft layer increase the loads at the beginning of the

impact stage and make the loads negative at the end of the impact stage.

Deflections of the ice plate are also affected by the viscous properties of both the ice and the soft layer, see Fig. 7. The symmetric deflections of the ice plate for the same impact conditions are compared for case 1 (left) without any viscosity in the system and case 4 (right) with $\tau_e = 0.1$ s and $\tau_i = 0.01$ s. The ice plate is relatively short in these calculations. Only the heavy rigid mode, $\psi_1(x)$, and the lowest even elastic mode, $\psi_3(x)$, are pronounced in the shapes of the plate shown in Fig. 7. The second even elastic mode, $\psi_5(x)$, can be recognized only for case 1 at $t = 0.015$ s. Vibrations of the plate are well pronounced. The plate becomes almost flat by the end of the impact stage in both cases.

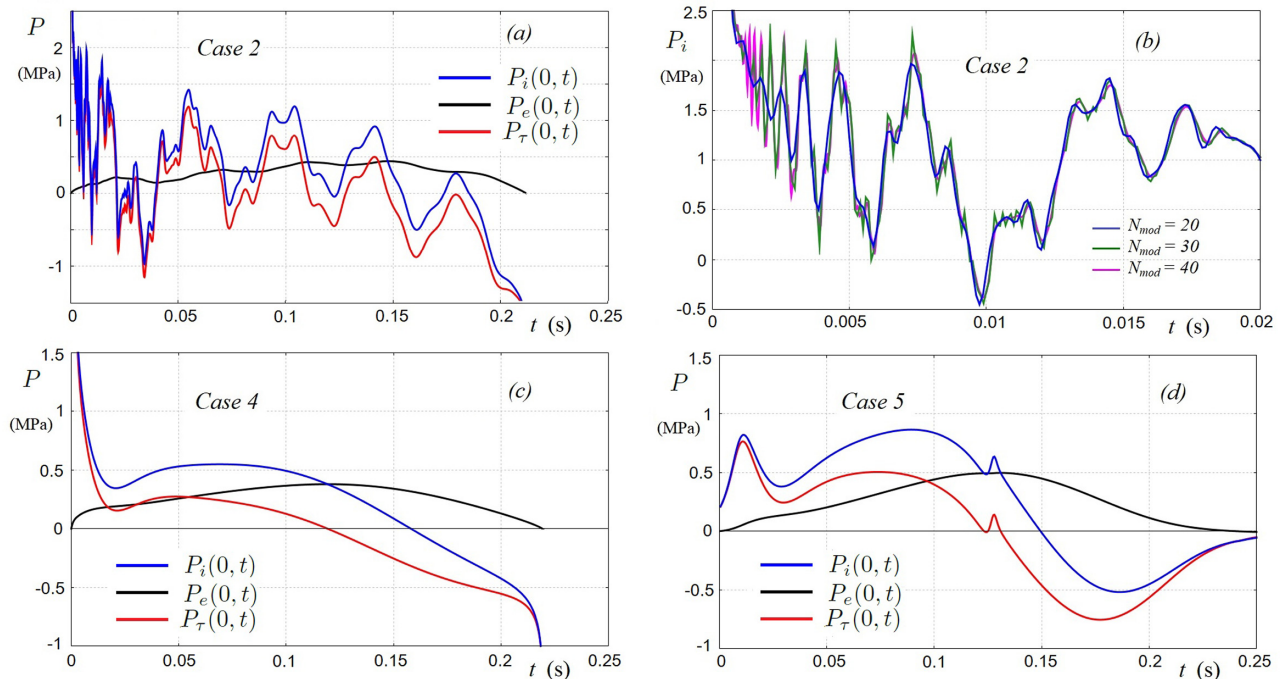


FIG. 5. Impact pressure $P_i(0, t)$ (blue lines) and its components $P_e(0, t)$ (black lines) and $P_\tau(0, t)$ (red lines) for cases 2 (a), 4 (c), and 5 (d). (b) $P_i(0, t)$ for case 2 calculated with 20, 30, and 40 modes at the very beginning of the impact.

Maximum strain magnitudes along the plate, $\max|\varepsilon(x, t)|$, where $|x| < L$, as functions of dimensional time are shown in Fig. 8 for cases 1–5 together with the positions along the plate, where the maximum strains are achieved. It is seen that the absolute maximum strains are achieved at the center of the plate at early stage, when the displacement of the rigid body is less than 10 cm. If $\max|\varepsilon(x, t)|$ is not achieved at the plate center, see Figs. 8(c) and 8(d), then the values of the strains are much smaller than the absolute maximum strains with the first elastic modes are not providing the major contribution. The strains are higher with stronger vibrations for $\tau_i = 0$. Figure 8(b) shows that the strains are weakly dependent on the characteristics of the soft layer.

The strains $\varepsilon(x, t)$ along the upper surface of the ice plate during the impact stage are shown in Fig. 9 for cases 1–5. The upper surface of the plate is in compression initially but then in tension because of the plate elastic vibration at the end of the impact stage. The strains are calculated even after the impact stage.

The coefficients of the rigid heave mode, $a_1(t)$, and two lowest elastic symmetric modes, $a_3(t)$ and $a_5(t)$, see equation (13), are shown as functions of time in Fig. 10(a) for cases 1, 2, and 4. The coefficients of higher elastic modes oscillate at higher frequencies with their magnitudes delaying quickly with the mode number, see Table II for magnitudes of elastic modes during the impact stage.

Strains $\varepsilon(x, t)$ at three points of the upper ice plate surface calculated for case 4 with 20 and 12 modes are shown in Fig. 10(b). This figure confirms good accuracy of the present calculations by the normal mode method.

One may conclude that the viscoelastic models of ice and the soft layer provide reliable strain distributions with 20 normal modes: 2 rigid, 9 even, and 9 odd elastic modes, for impact conditions of this subsection.

In the following subsections, strains in the ice plate are investigated for case 4 ($\tau_i = 0.01$ s, $\tau_e = 0.1$ s, and $K = 1$ MPa) and different impact speeds, plate length, and thickness.

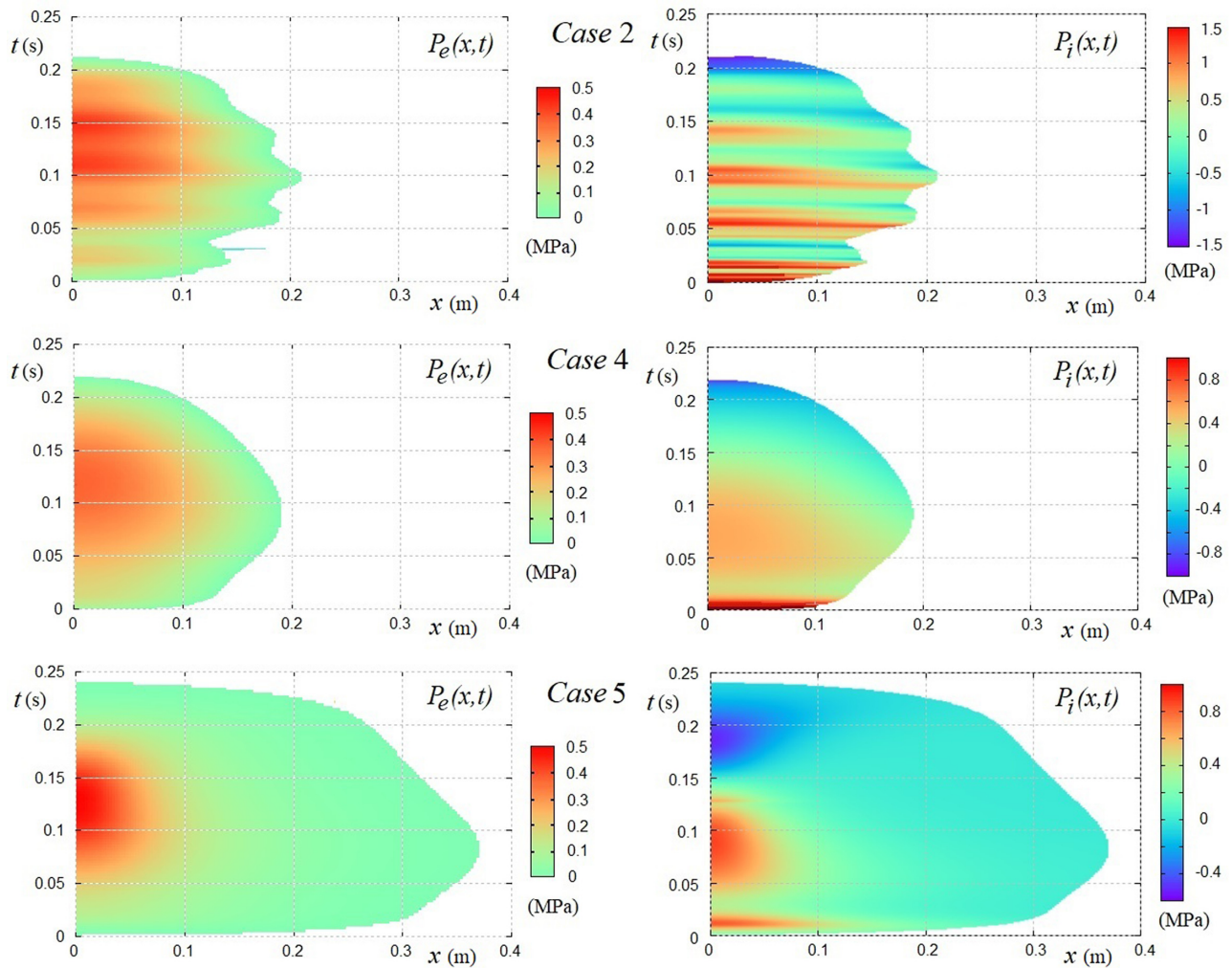


FIG. 6. Elastic component $P_e(x, t)$ (left) and the total impact load $P_i(x, t)$ (right) in cases 2, 4, and 5.

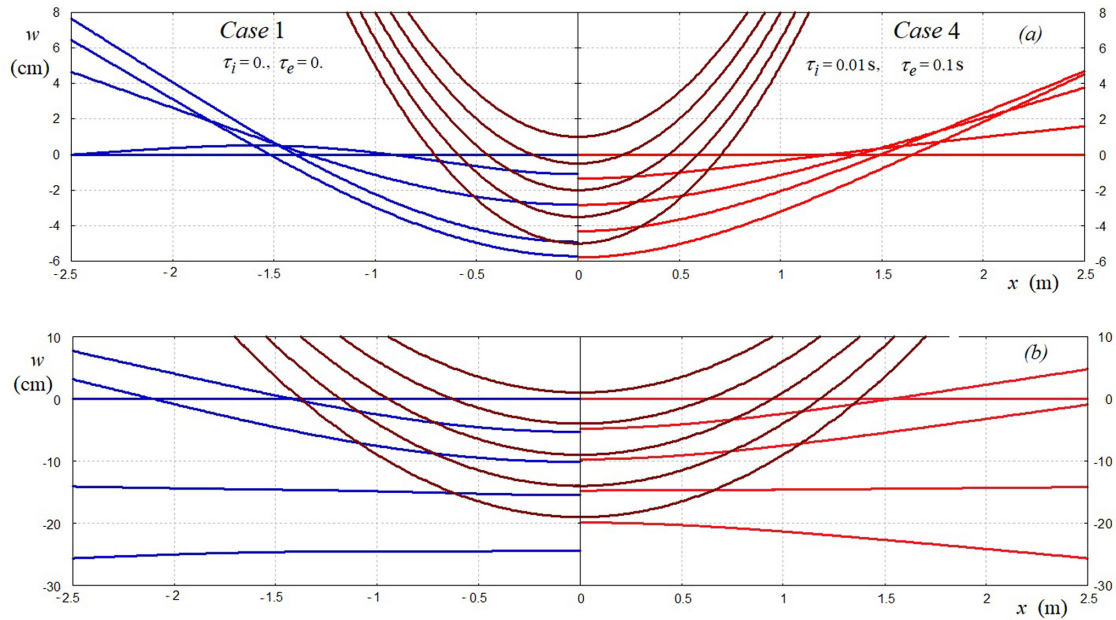


FIG. 7. Positions of the body surface and deflections of the ice plate in case 1 (left) and case 4 (right) for time instants $t = 0, 0.015, 0.03, 0.045, \text{ and } 0.06 \text{ s}$ (a), and $t = 0, 0.05, 0.1, 0.15, \text{ and } 0.2 \text{ s}$ (b).

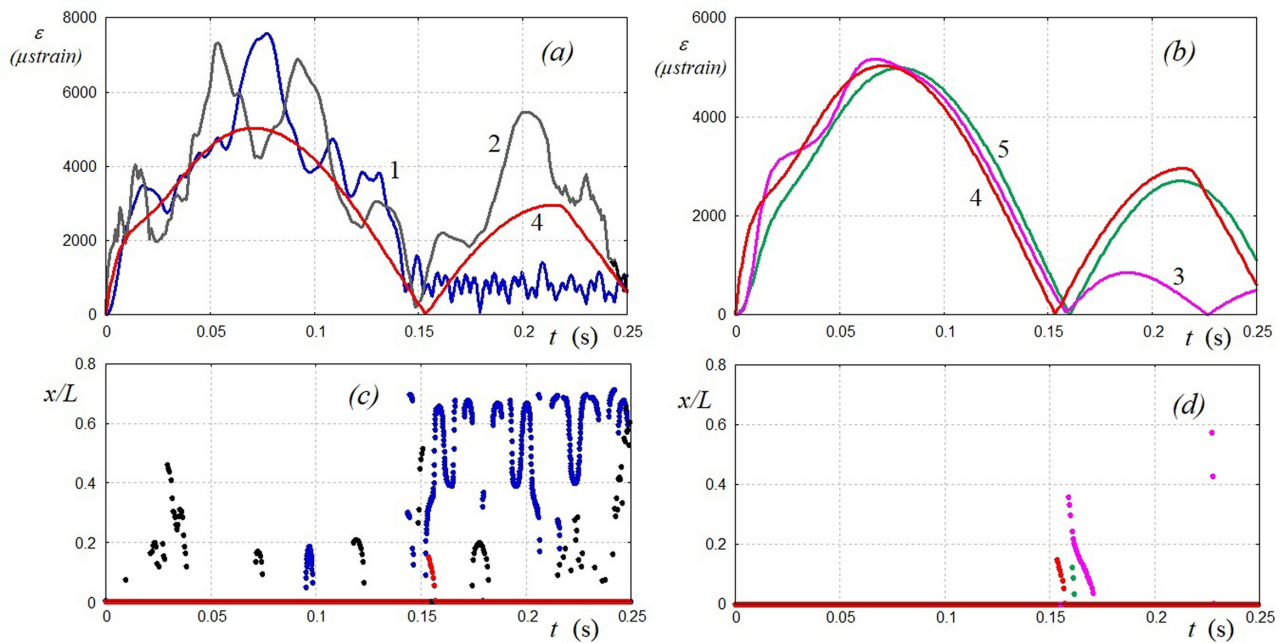


FIG. 8. Maximum strain magnitudes along the plate, $\max|\epsilon(x, t)|$, where $|x| < L$, for cases 1, 2, and 4 (a) and 3, 4, and 5 (b) together with the positions where the maximum strains are achieved, (c) and (d) correspondingly.

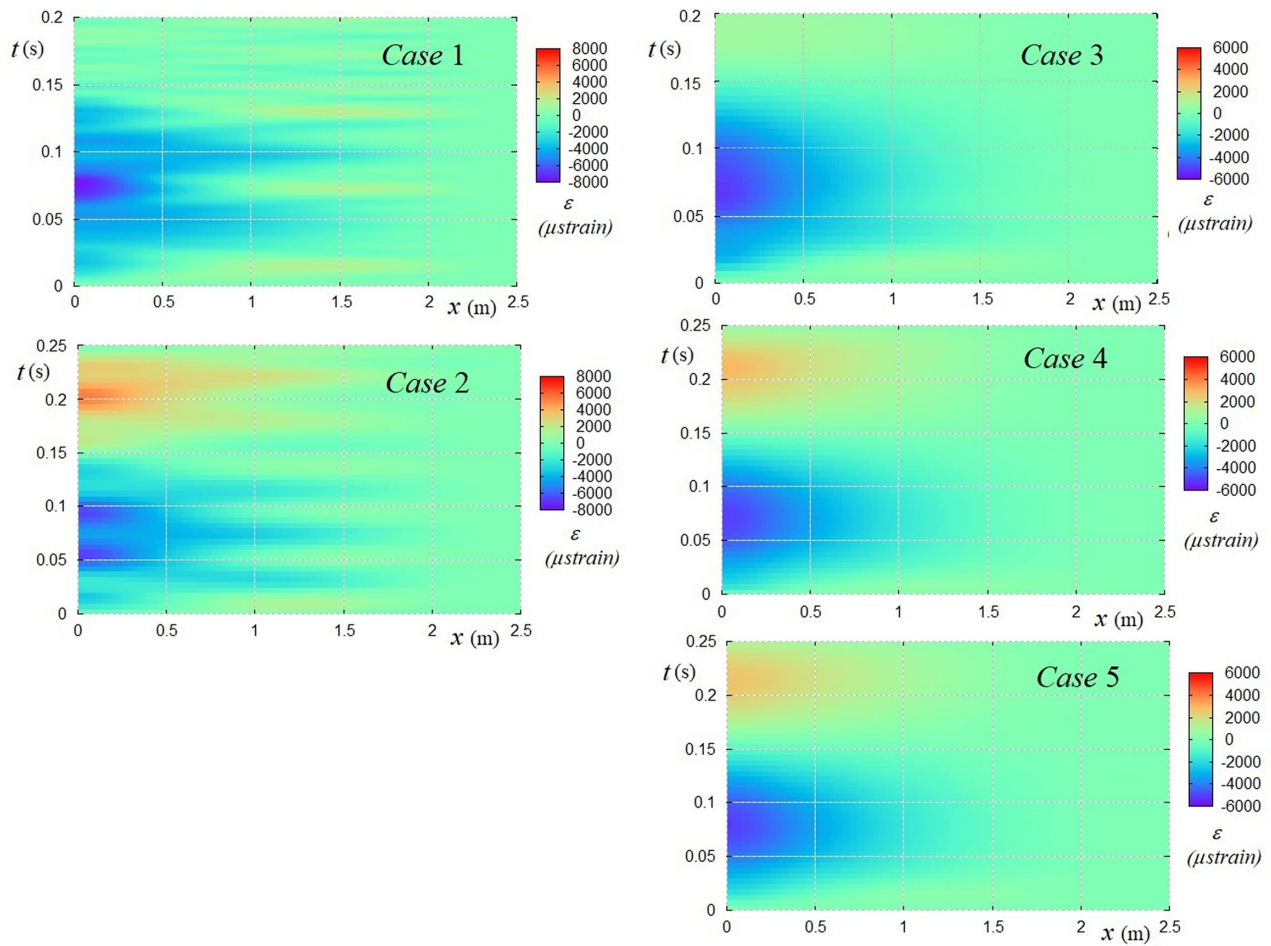


FIG. 9. The strains $\varepsilon(x, t)$ along the upper surface of the ice plate during the impact stage in cases 1–5.

B. Maximum strains in ice plate

In this section, we investigate maximum strain magnitudes,

$$\varepsilon_{\max}(t) = \max_{0 \leq x \leq L} |\varepsilon(x, t)|,$$

as functions of time in the viscoelastic ice plate depending of plate thickness h_i , plate length L , and impact velocity V . Calculations of the

strains $\varepsilon(x, t)$ are performed by formula (25) with 20 modes. It will be shown that the scaled maximum strain

$$\hat{\varepsilon}_{\max}(\hat{t}) = \frac{h_i V_p}{LV} \varepsilon_{\max}, \quad V_p = \sqrt{\frac{E}{\rho_i}}$$

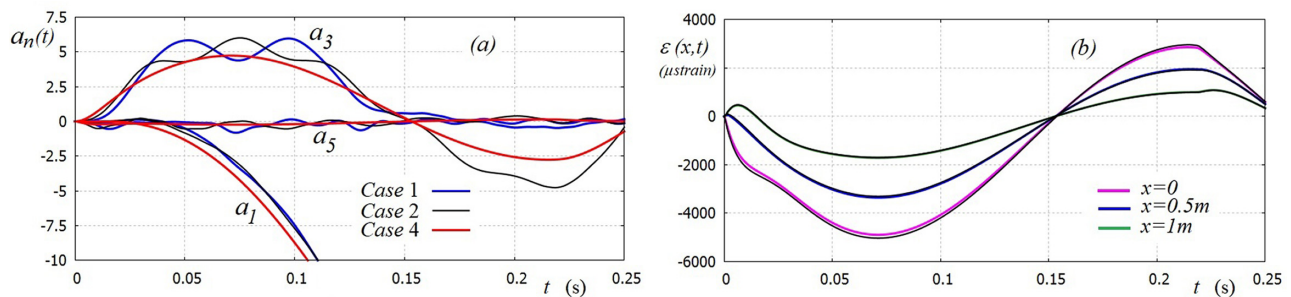


FIG. 10. (a) Coefficients $a_n(t)$ of the modes with $n = 1, 3,$ and 5 as functions of time in cases 1 (blue lines), 2 (black lines), and 4 (red lines). (b) Evolutions of the strains $\varepsilon(x, t)$ at three points, $x = 0, 0.5,$ and 1 m, of the upper ice plate surface in case 4 calculated with 20 modes (colored lines) and 12 modes (black lines).

TABLE III. Natural periods of the first wet mode T_1 for different plate thickness and plate length.

h_i (m)	L (m)	T_1 (s)
0.10	2.5	0.25
0.15	2.5	0.143
0.20	2.5	0.098
0.25	2.5	0.073
0.30	2.5	0.058
0.15	1.5	0.0455
0.15	2	0.085
0.15	2.5	0.143
0.15	3	0.22
0.15	3.5	0.318
0.25	3	0.1115
0.10	2	0.147

as a function of the scaled time $\hat{t} = t/T_1$ is weakly dependent on the impact conditions. The periods of the first natural wet mode T_1 for different thickness and length of the floating ice plate are shown in Table III.

The strains $\varepsilon_{\max}(t)$ and $\hat{\varepsilon}_{\max}(\hat{t})$ are depicted for the impact speed of 1 m/s and different plate thickness, Fig. 11, and plate length, Fig. 12. The figures show that the scaled strains weakly depend on the parameters of the ice plate. These strains for different impact speeds and a plate length of 5 m and a thickness 15 cm are shown in Fig. 13. Finally, three mixed cases are shown in Fig. 14, justifying that the introduced

scaled strains as functions of the scaled time correctly describe the dependence of the strains in the ice plate on the parameters of impact. Note that $\hat{\varepsilon}_{\max}(\hat{t})$ is smaller than 0.7, which gives the following estimate of the strains in μs :

$$|\varepsilon(x, t)| < 0.7 \times 10^6 \frac{LV}{h_i V_p}.$$

The yield strain is equal to $80 \mu\text{s}$ for ice. Therefore, a floating ice plate would not be cracked by impact if the impact conditions satisfy the inequality $LV/h_i < 114V_p \times 10^6$. For the Young's modulus of the ice $E = 4.2 \times 10^9 \text{ Pa}$ and the density of ice $\rho_i = 917 \text{ kg/m}^3$, we have $V_p = 2140 \text{ m/s}$, and the condition of no damage to the ice plate becomes $V < (h_i/L) \times 0.24 \text{ m/s}$. In the theory of thin plate, the ratio h_i/L should be smaller than 1/10 at least. Therefore, a thin ice plate is not broken by an impact only if the impact speed is smaller than 2 cm/s. For the upper limit, $1000 \mu\text{s}$, of the yield strain for ice, see Schulson (1999), the limiting impact speed increases up to 0.3 m/s. We conclude that long ice plates are unlikely to survive vertical impacts at constant speeds. The long ice plates break into initially two and then possibly even more shorter plates, each of them can be modeled as viscoelastic thin but shorter plate. These shorter plates are more likely to survive during the continuing interaction with the impacting body. If some of these shorter plates are very short, then they can be treated as rigid plates, see Khabakhpasheva et al. (2018b). Criteria of the ice plate cracking are not certain and depend on particular ice type and the applied load. Once a crack is initiated, it decreases the loads in the ice plate and can grow if the stresses in the plate are still large. The present results, see Fig. 9, suggest that the first crack starts from the lower surface of the plate and propagates toward the upper surface of the plate,

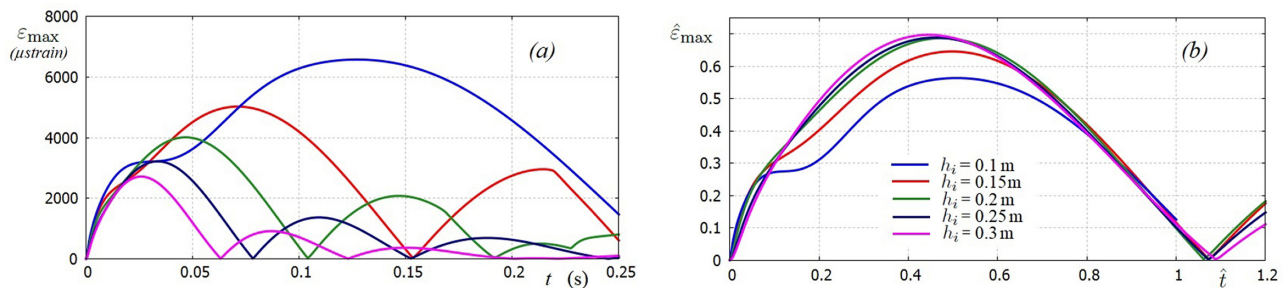


FIG. 11. Maximum strains $\varepsilon_{\max}(t)$ (a) and $\hat{\varepsilon}_{\max}(t)$ (b) for $h_i = 0.1, 0.15, 0.2, 0.25,$ and 0.3 m , $L = 2.5 \text{ m}$, and $V = 1 \text{ m/s}$. Colors of lines are the same in (a) and (b).

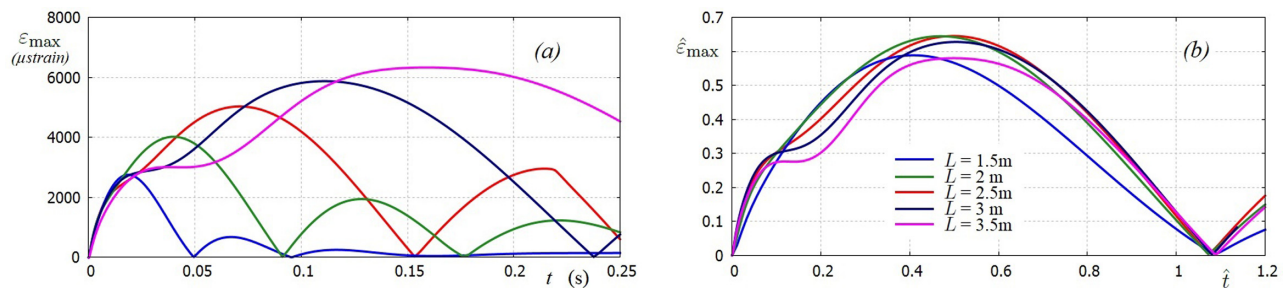


FIG. 12. Maximum strains $\varepsilon_{\max}(t)$ (a) and $\hat{\varepsilon}_{\max}(t)$ (b) for $L = 1.5, 2, 2.5, 3,$ and 3.5 m , $h_i = 0.15 \text{ m}$, and $V = 1 \text{ m/s}$. Colors of lines are the same in (a) and (b).

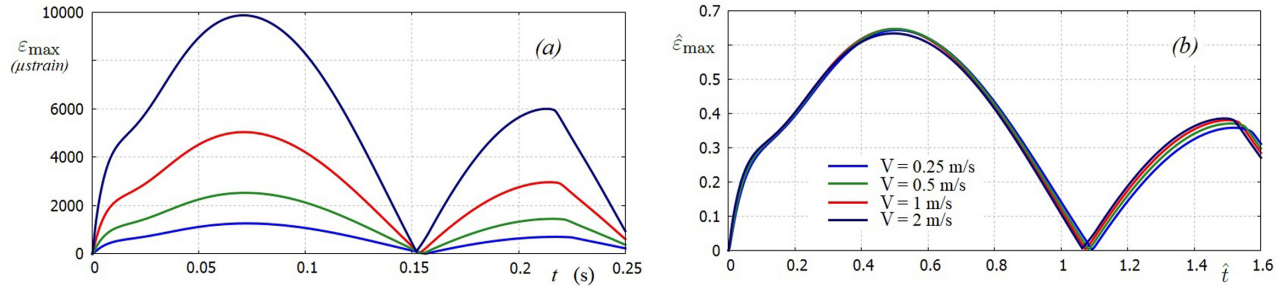


FIG. 13. Maximum strains $\epsilon_{\max}(t)$ (a) and $\hat{\epsilon}_{\max}(t)$ (b) for $V = 0.25, 0.5, 1,$ and 2 m/s, $h_i = 0.15$ m, and $L = 2.5$ m. Colors of lines are the same in (a) and (b).

breaking finally the plate into two ones if the load is strong enough, see Korobkin and Khabakhpasheva (2018) for a model of crack propagation through the thickness of a floating plate.

C. Rigid body impact onto long ice plates

Figure 7 with deflections of an ice plate caused by a rigid body impact demonstrates that only lowest elastic modes are important for relatively short plates. Both plate deflections and bending stresses in the plate behave differently for longer plates. We may expect that the plate deflections near the impact place are weakly dependent on the plate length. However, at a distance from the impacting body, the plate length plays the major role.

We are concerned with long and thin plates in this section. Calculations are performed for ice thickness $h_i = 10$ cm, thickness of the soft layer $h_e = 1$ cm, rigidity coefficient of the soft layer $K = 1$ MPa, radius of the curvature of the rigid body surface $R = 5$ m, retardation time of ice $\tau_i = 0.01$ s, and retardation time of the soft layer $\tau_e = 0.1$ s. The impact speed is 1 m/s in all calculations of this section. The number of the retained normal modes, $N_{mod} = 49$, was found to be suitable for accurate describing interaction between water, floating ice plate, and the impacting body for ice plates with a length up to 40 m. The longer the plate, the more modes should be retained.

Deflections of ice plates with lengths $L = 20, 30,$ and 40 m and an impact at the plate centers are shown in Fig. 15(a) at time instants $t = 0.5, 1, 1.5,$ and 2 s. Near the body, the deflections are close to each other, but far from the body, the deflections are very different. Figure 15(b) shows deflections for plates with lengths 10 and 20 m, where $|x| < 12.5$ m. Edge effect is strong for the short plate even near the

body. Strains on the lower surface of the plate are shown in Fig. 15(c) at $t = 1$ and 2 s for $L = 20$ and 40 m. In contrast to the deflections, the strains are sensitive to the plate length even near the body surface. The maximum strain is achieved at the impact point $x = 0$, where the shape of the plate approaches the shape of the rigid body. The strain at a point on the surface of the ice plate is equal to half-thickness of the plate $\frac{1}{2} h_i$ multiplied by the plate curvature at this point. The plate curvature at the impact point approaches the curvature of the body, which provides the estimate of the strain $10\,000$ μ strain. Compare this estimate with the calculated strain at the plate center at $t = 2$ s.

The strains $\epsilon(0, t)$ at the plate center as functions of dimensional time for plates of lengths 10, 20, 30, and 40 m are shown in Fig. 16. All lines approach $10\,000$ μ strain, which corresponds to the radius of curvature of the impacting body. The shorter the plate, the higher the strain vibrations.

Figures 17–19 show deflections of the plate and strains along the lower surface of the plate with a $L = 20$ m impacted at different places. Other parameters of impact are given at the beginning of this subsection. Figures 17–19(a) and 19(b) are for the early stage of impacts, and Figs. 17–19(c) and 19(d) are for the later stage. It is seen that this long ice plate does not bounce from the body surface with time as for a shorter plate in Fig. 7. The higher elastic modes provide important contributions to both deflections and strains during the early stage, see Figs. 17–19(a) and 19(b), but they are less important at the later stage, when high-frequency vibrations of the plate decay because of viscous properties of the ice. Figures 17(d) and 18(d) show that the strains achieve their maximum value $10\,000$ μ strain at the impact point. The strains are smaller for the impact close to the plate edge, see Fig. 19(d). It is interesting to note that both the deflections and strains are

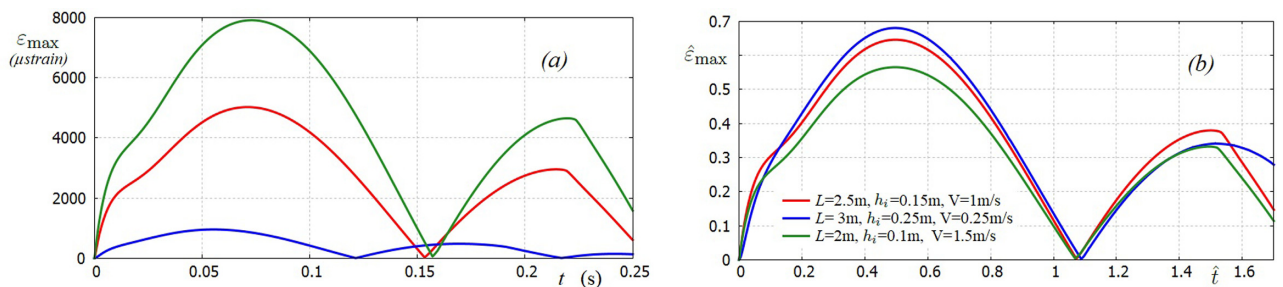


FIG. 14. Maximum strains $\epsilon_{\max}(t)$ (a) and $\hat{\epsilon}_{\max}(t)$ (b) for three cases specified in (b). Colors of lines are the same in (a) and (b).

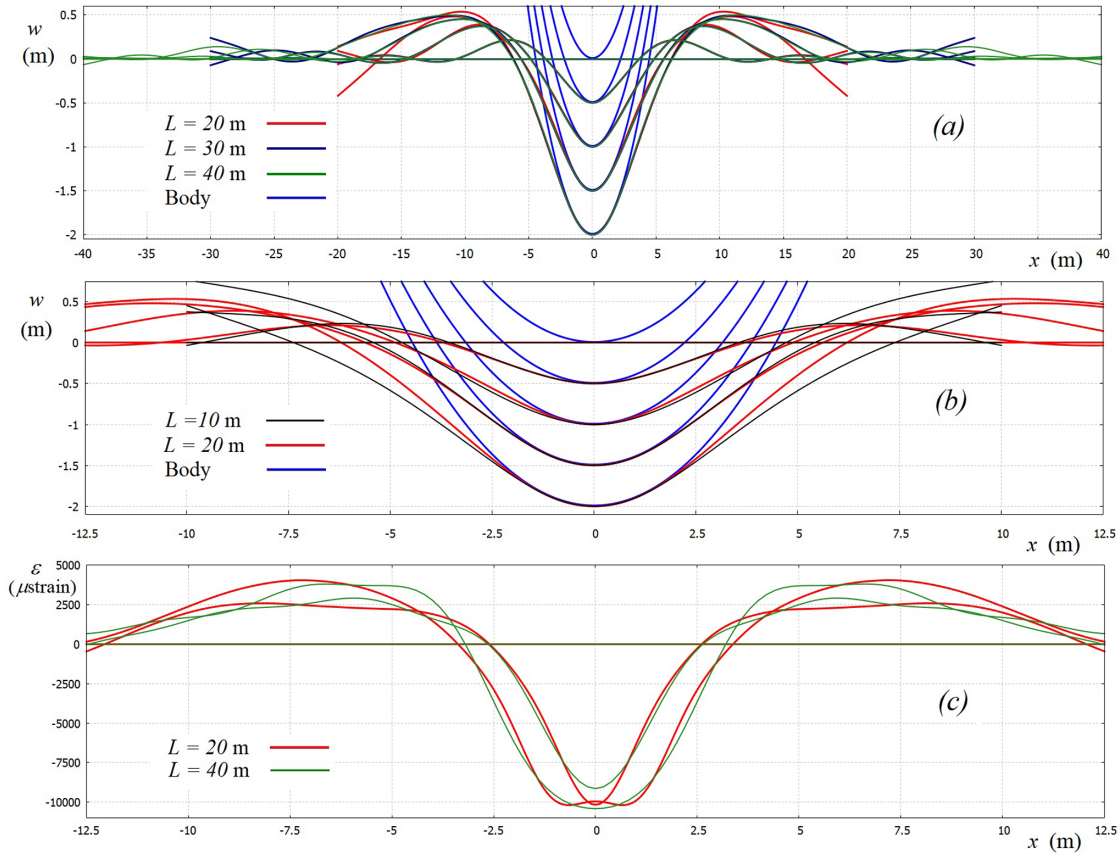


FIG. 15. (a) Positions of the body (blue lines), and deflections of the plates with lengths of 20 m (red lines), 30 m (deep blue lines), and 40 m (green lines) at time instants $t = 0, 0.5, 1, 1.5,$ and 2 s. (b) Closed view of the plate deflection near the body surface for plate lengths of 20 m (red line) and 10 m (black line). (c) Strains on the lower surface of the plate lengths of 20 m (red lines) and 40 m (green lines) at $t = 1$ and 2 s.

relatively small in the main part of the plate for impact close to the plate edge, see Fig. 19. However, the deflections at another edge of the plate are of the order of the body displacement during the early stage, see Fig. 19(a). This effect can be explained by the flexural waves, see Morse (1948), generated by the impact and propagating along the plate toward another edge of the plate. Reflection of dispersive flexural wave from the plate free-free edge increases the deflection of the edge.

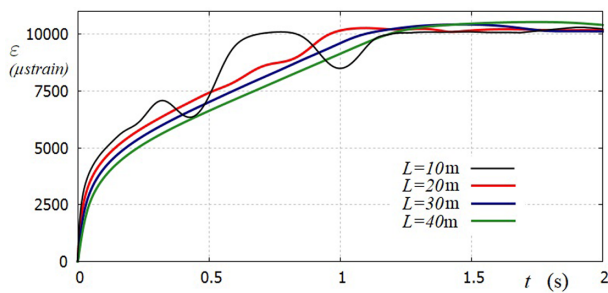


FIG. 16. Strains at $x = 0$ as functions of time for $L = 10, 20, 30,$ and 40 m.

Morse (1948) studied flexural waves in an Euler beam of infinite length caused by an initial deflection of the beam. To support our finding about large deflection of the opposite edge of the plate, we calculated unsteady response of the plate as in Figs. 17–19 but placed on a soft elastic foundation. A point load of the constant magnitude was applied instantly at the right edge of the plate. It was shown that the maximum deflection of the left edge of the plate occurs shortly after the impact and is just 10% smaller than the plate deflection at the edge of the impact. In contrast, the maximum deflection of the center of the plate is twice smaller than the deflection at the impact edge. Similar results are reported on hydroelastic response of a ship segmented model subject to bow-flare slamming measured in model experiments, see Jiao and Ren (2016). The measured accelerations of the model bow due to slamming loads were of order of 4 m/s^2 , and the measured accelerations of the model stern caused by whipping were of order of 2 m/s^2 , see Fig. 10 in Jiao and Ren (2016). The free-free ends of the ship segmented model vibrated at higher amplitude than the inner part of the model. Figure 19(a) shows the plate deflections shortly after the impact on the right edge of the plate. If there is no damping in the floating plate, then the flexural waves generated by the impact on the right edge propagate toward the left edge with its amplitude decaying

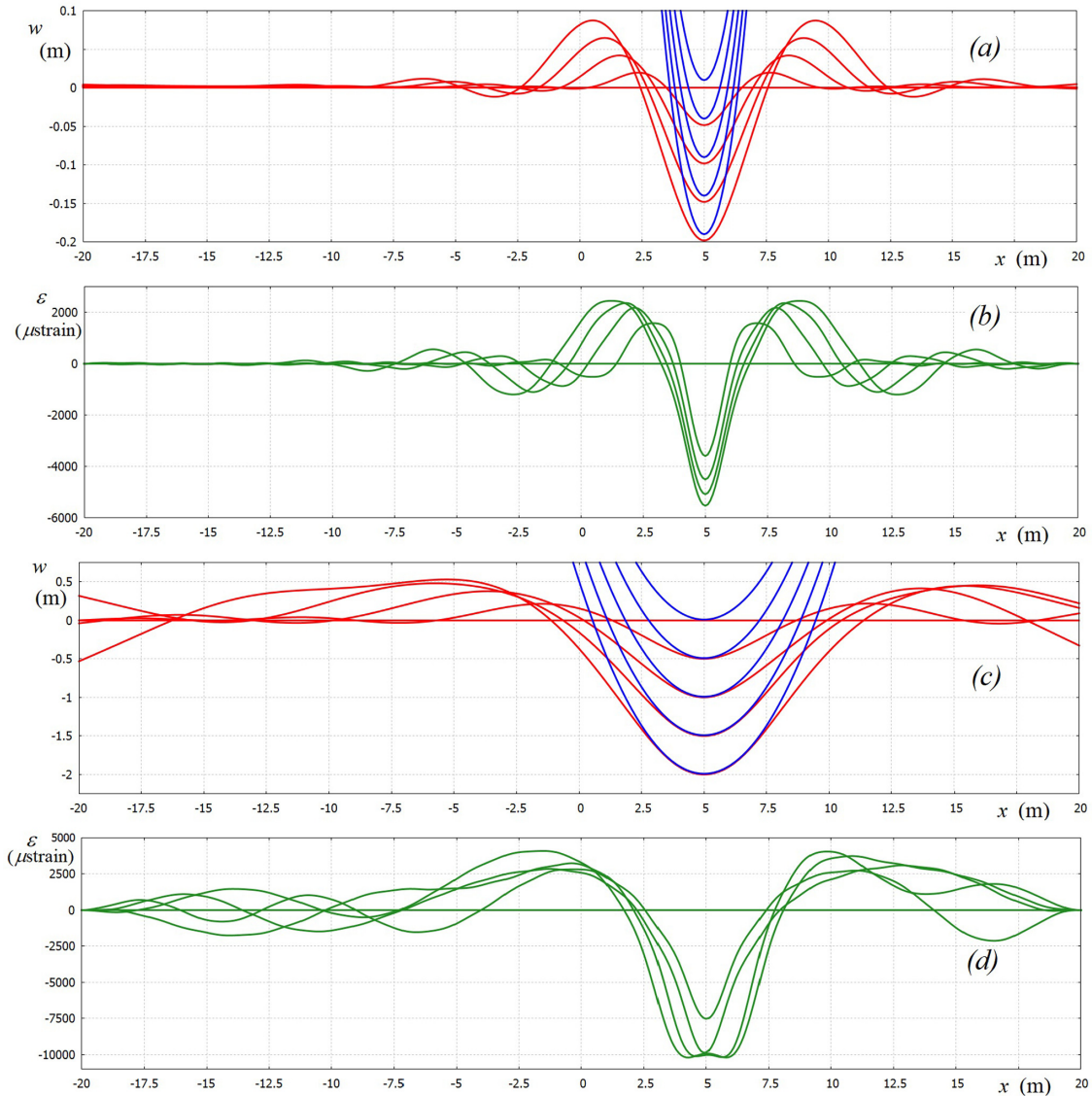


FIG. 17. Impact at $x = 5$ m. Deflections (a) and strains (b) at $t = 0.05, 0.1, 0.15,$ and 0.2 s (c). Deflections (c) and strains (d) at $t = 0.5, 1, 1.5,$ and 2 s. Deflections are shown by red lines, the body positions by blue lines, and the strains are by green lines.

only due to dispersion of the waves. It is interesting that a sinusoidal wave propagating along a dry semi-infinite free-free beam from infinity toward the edge of the beam causes deflection of the edge, which is $2^{\frac{3}{2}}$ times greater than the amplitude of the incident wave. Viscous properties of the plate force the disturbances due to the impact decay with a distance from the place of the impact. However, the results shown in Figs. 17–19 are obtained for small retardation time, $\tau_i = 0.01$ s. For larger retardation times of the floating plate, the plate deflections are expected to be more visibly localized near the impact place.

Strains at different points of the initial impact are shown in Fig. 20. The strains are close to each other for $|x_0| \leq 0.5L$. For impacts far from the edges, the shape of the plate approaches the body shape near

the impact place, see Figs. 15, 17, and 18. If the impact occurs close to the plate edge, the strains become smaller initially but then grow in time.

V. CONCLUSION

Two-dimensional impact of a rigid body onto a floating ice floe has been studied with a focus on relatively long plates and blunt convex bodies. The hydrodynamic loads, ice deflection, bending stresses in the ice plate, and the impact loads are determined simultaneously during the initial stage of impact, when the ice and body displacements are small, but the bending stresses in the ice are maximum. A thin viscoelastic layer was placed on the top of the floating plate to model the properties of the ice surface including a layer of snow or crushed ice

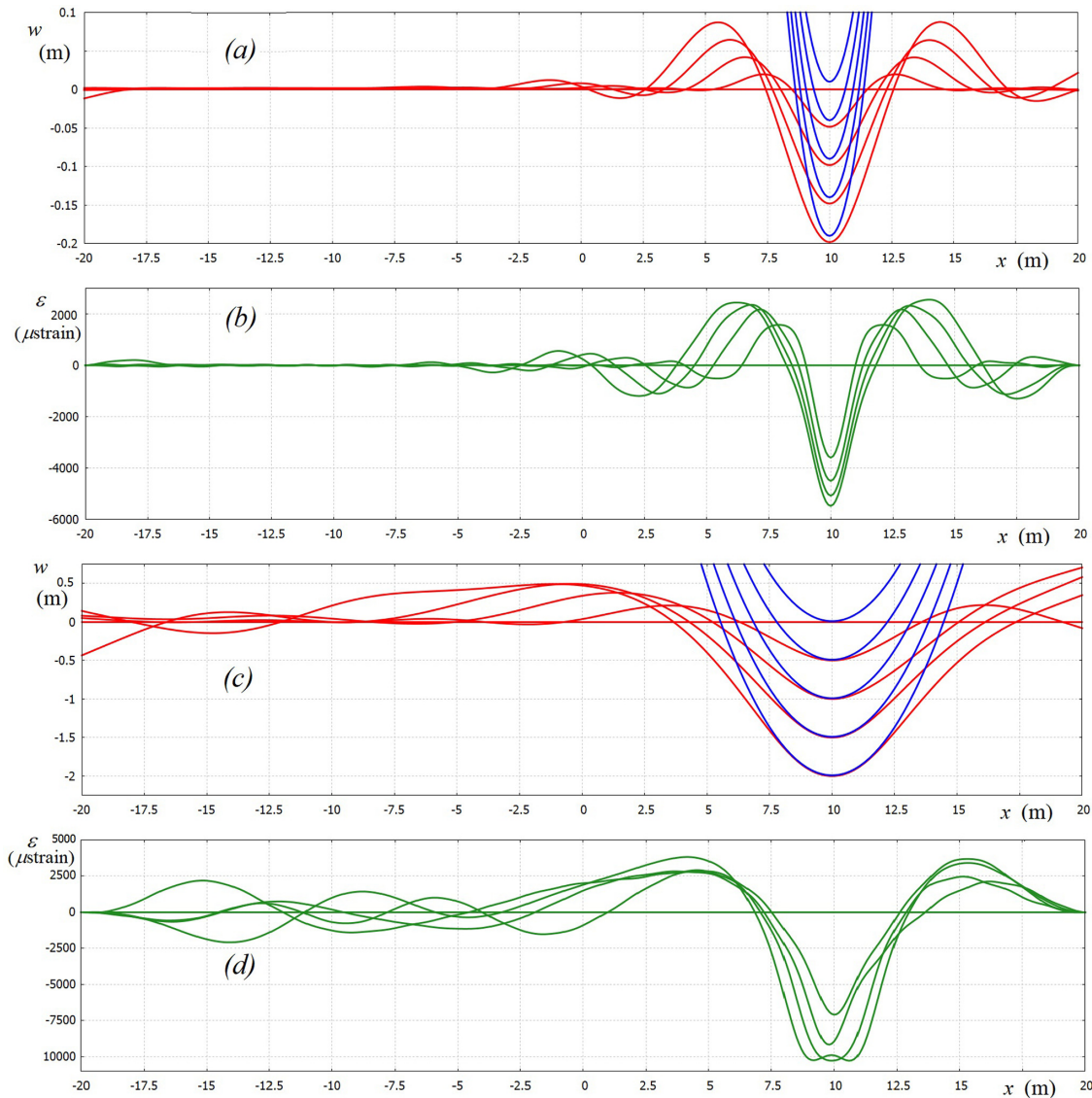


FIG. 18. Impact at $x = 10$ m. Deflections (a) and strains (b) at $t = 0.05, 0.1, 0.15,$ and 0.2 s (c). Deflections (c) and strains (d) at $t = 0.5, 1, 1.5,$ and 2 s.

crystals. The flow of the liquid caused by the ice plate deflection is described by the linearized potential flow theory during this early stage. The ice plate deflection is calculated by the normal mode method.

It was shown that the soft layer does not significantly affect the stresses in the ice plate and plate deflection but, on the other hand, make calculations of the impact loads regularly. Viscous properties of the soft layer allow to describe the interaction of the rigid body with floating ice in a more realistic way without multiple bouncing of the ice from the impacting body. Nevertheless, the ice plate finally separates from the body surface after a short impact stage due to elastic oscillation of the plate. This is a non-obvious effect. The model of inelastic collision on a floating body, see Joukowski (1884), which was

used by Khabakhpasheva *et al.* (2018b) for short ice floes with negligible elastic motions, suggests that the separation of two impacting bodies is governed by the rate of impact energy dissipation in a soft layer between the bodies. The present results showed that impacting bodies may separate if at least one of the bodies is elastic and vibrates because of the impact.

Viscous properties of the soft layer increase significantly the initial impact loads and make them negative near the end of the impact stage. As a result of large and concentrated impact loads, the plate vibrates initially at a high frequency. However, shortly after this early stage, these vibrations vanish because of viscosities of both the soft layer and the ice plate. It is not intuitively clear that a viscoelastic cover, which could be designed to mitigate impact loads, increases the

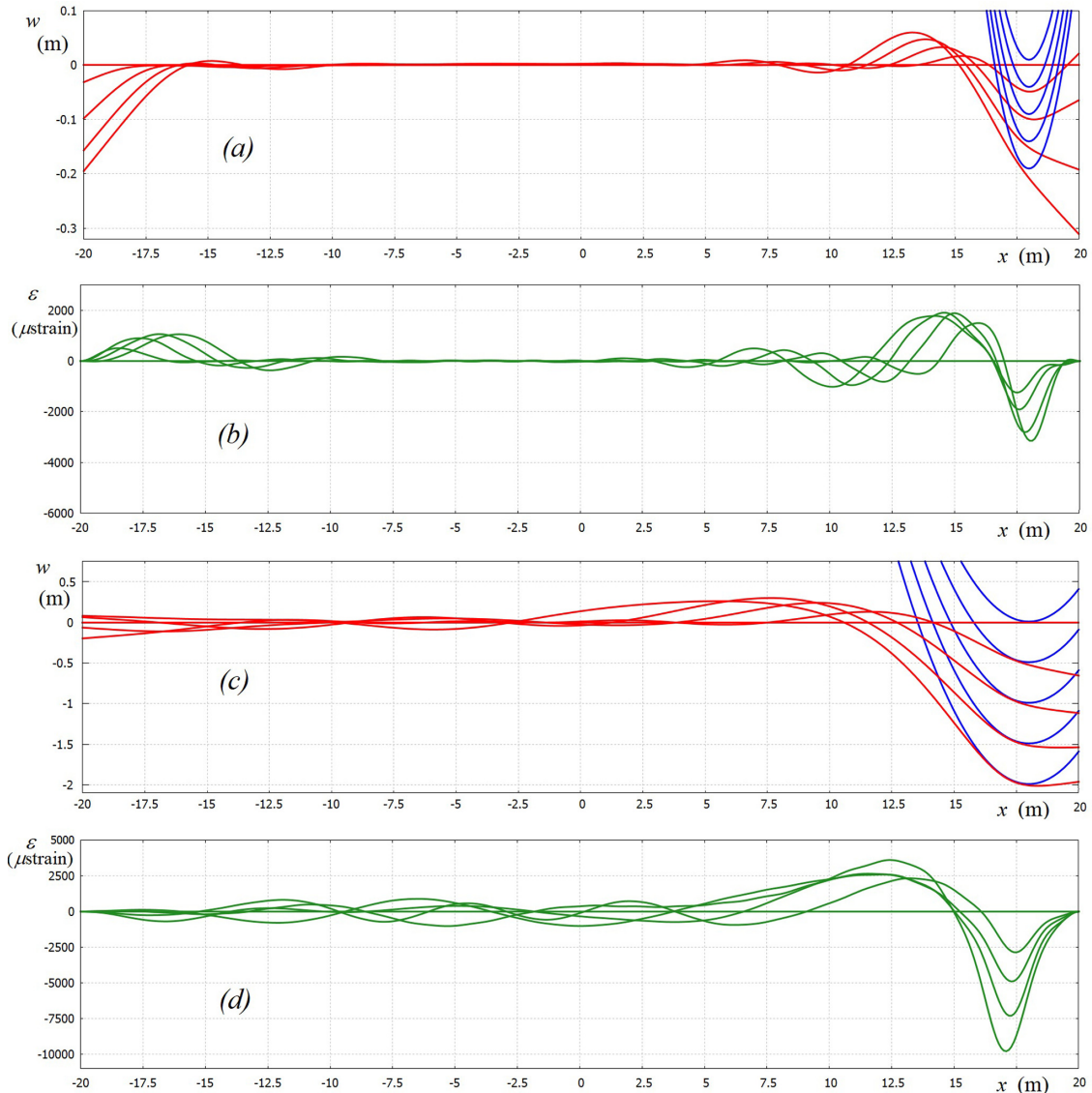


FIG. 19. Impact at $x = 18$ m. Deflections (a) and strains (b) at $t = 0.05, 0.1, 0.15,$ and 0.2 s (c). Deflections (c) and strains (d) at $t = 0.5, 1, 1.5,$ and 2 s.

loads because of viscous properties of the cover. Viscous characteristics of the cover play different roles for slow and impulsive loading. Roughly speaking, a viscoelastic cover is “more rigid” for impulsive loads than just a corresponding elastic cover. Another surprising effect of viscous properties of the cover was observed at the end of the impact stage before the elastic plate separates from the impacting rigid body. The viscous effects lead to tensile stresses in the cover, which do not occur for elastic cover, see Fig. 5. During the main part of the impact stage, the deflections of the ice plate and the strains in it are well described with few lowest modes of the dry plate vibration.

The maximum strains along the plate were analyzed as functions of time for central impacts. It was shown that the maximum strains are proportional to the impact speed and length of the plate, and

inverse proportional to the plate thickness. The evolution of the correspondingly scaled strains is well described using the dimensionless time, where the timescale is the period of first wet mode of the plate. The absolute maximum of the scaled strains was found to be 0.7 for the considered range of impact conditions. Note that the strains in the viscoelastic plate peak during the impact stage before the plate separates from the impacting body, see Fig. 9. Free vibration of the plate after the separation releases the strains.

Impact at any point of the floating plate was studied for relatively long and thin plates. Such plates are flexible. Large number of modes is required to describe the strains in such plates accurately during the early stage. The maximum strain in the plate was shown to be achieved at the impact point, if the impact occurs far enough from the plate

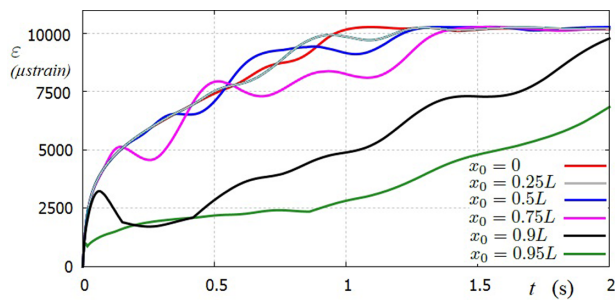


FIG. 20. Strains at different points of the initial impact, $x = x_0$, as functions of the dimensional time for a plate length $2L = 40$ m and $x_0 = 0, 5, 10, 15, 18,$ and 19 m.

edges, and to be weakly dependent on viscoelastic properties of the soft layer. The maximum strain corresponds to the plate deflection, where the plate shape approaches the shape of the impacting body. The strains are smaller than the yield strain for the ice, only for either very low speeds of impact or small curvature of the rigid body surface. If the impact occurs close to the plate edge, then the edge penetrates deep into water, and the presence of water on the upper surface of the plate, as well as the direct interaction of the water with the body surface, should be included in the model.

The present model makes it possible to investigate the ice response to impact on its surface in a wide range of impact conditions. The model can be used also for analysis of impacts onto artificial floating thin structures. The theoretical predictions of the present model were compared with the CFD results in Korobkin *et al.* (2020). The Navier-Stokes equations are solved numerically with a finite-volume method from the OpenFOAM opensource CFD software. The hydrodynamic pressure is calculated with the CFD solver that uses a deforming mesh method to account for the deflection of the ice plate. The CFD solution is discrete in space and time, whereas the structural modal model is discrete in time, but uses a basis of continuous mode shapes. Due to the finite representation of the spatial discretization, the CFD solution effectively limits the number of structural modes that can be used. The CFD results are presented in Fig. 10 for the deflection of the viscoelastic plate impacted at the center by a rigid body, and for the pressure distribution in the liquid under the plate. The CFD results showed that the pressure along the ice/water interface can be higher and lower than the atmospheric pressure. However, the total pressure is still higher than the vapor pressure for water, which is about 0.6 kPa at 0 °C temperature.

The predictions by the present linearized hydrodynamic model were compared with the CFD results by Khabakhpasheva *et al.* (2018b), see Fig. 5 in this paper, for short floating plates and free falling body. It was shown that theoretical and numerical predictions of the body and plate displacements, velocities, and accelerations during the impact are very close to each other. This indicated that the linearized hydrodynamic model can be used for predictions of motions during the short impact stage.

The model will be developed further by including preexisting and new cracks on the plate surface, with a growth of the cracks in time up to complete breaking of the plate into two parts. The obtained results showed that the impact onto a floating ice floe at a constant speed always generates strains in the ice floe, which are higher than the yield strain value. We may conclude that the highest deceleration of a free

fall lifeboat occurs during the initial short impact stage, when the ice floe is still continuous. Zakki *et al.* (2016) wrote about lifeboat launching on open water “The international regulations require that a lifeboat for free fall launching should be able to give protection against impact accelerations when it is launched with its full occupants and equipment from at least the maximum designed height. Since the height of offshore structure to the water surface is significantly high, during the water entry phase the acceleration response of the free fall lifeboat might cause an injury to the occupants. The special hull form design should be applied to reduce the acceleration.” How to use conventional lifeboat in icy waters is still an open question. Some recommendations were given by Maki *et al.* (2017), Khabakhpasheva *et al.* (2018b), and Chen *et al.* (2019) by both CFD and theoretical analysis, who showed that free fall launching without direct contact of the lifeboat with ice floes is safe; the increase in the lifeboat deceleration caused by floating ice floes is less than 5% if the gap between the lifeboat and the nearest ice flow is greater than 1/5 of the lifeboat beam, see Fig. 2 in Khabakhpasheva *et al.* (2018a). The corresponding estimates of the maximum lifeboat deceleration in the case of the boat impact with an ice floe have not been obtained so far. We expect that helpful recommendations about the design of lifeboats for icy waters can be derived using the present model in terms of the thickness of ice floe and its dimension for safe launching of the boat. To arrive at such recommendations, the present model should be extended to include free fall of the body, as it was done in Khabakhpasheva (2018b), and crack propagation, as in Korobkin and Khabakhpasheva (2018). The viscoelastic model of ice should be more practical including the techniques to determine the ice characteristics in field conditions, see Marchenko *et al.* (2021) for such models and techniques.

The presented model can be developed further to include crashing of ice in the impact place in a one-dimensional way introducing a front of crushing and its dynamics depending on the impact loads. Available ice impact models including ice crushing were reviewed by Kim (2014). We expect that ice crushing by the impact of a rigid body with a small curvature of its surface will be less pronounced than for small indentors, and crushing can be reasonably well described using 1D approximation.

AUTHORS' CONTRIBUTIONS

All authors contributed equally to this work.

ACKNOWLEDGMENTS

This work was supported by the NICOP research grant “Vertical penetration of an object through broken ice and floating ice plate” N62909-17-1-2128.

DATA AVAILABILITY

The data that support the findings of this study are available within the article.

REFERENCES

- Bratov, V., and Petrov, Y., “Application of incubation time approach to simulate dynamic crack propagation,” *Int. J. Fracture* **146**(1), 53–60 (2007).
- Brocklehurst, P., Korobkin, A. A., and Parau, E. I., “Hydroelastic wave diffraction by a vertical cylinder,” *Philos. Trans. R. Soc. London A* **369**(1947), 2832–2851 (2011).

- Chen, Y., Khabakhpasheva, T., Maki, K. J., and Korobkin, A., "Wedge impact with the influence of ice," *Appl. Ocean Res.* **89**, 12–22 (2019).
- Conley, J. A., An Examination of a Subsurface Impact on a Floating Ice Sheet (Naval Surface Warfare Center Carderock Division, Bethesda, MD, 1997).
- Faltinsen, O. M., Kvelsvold, J., and Aarsnes, J. V., "Wave impact on a horizontal elastic plate," *J. Mar. Sci. Technol.* **2**(2), 87–100 (1997).
- Faltinsen, O. M., Landrini, M., and Greco, M., "Slamming in marine applications," *J. Eng. Math.* **48**(3), 187–217 (2004).
- Gerritsma, J., and Beukelman, W., "Analysis of the modified strip theory for the calculation of ship motions and wave bending moments," *Int. Shipbuilding Prog.* **14**(156), 319–337 (1967).
- Greenhow, M., "Wedge entry into initially calm water," *Appl. Ocean Res.* **9**(4), 214–223 (1987).
- Gudmestad, O. T., and Solberg, K. E., "Findings from two Arctic search and rescue exercises north of Spitzbergen," *Polar Geography* **42**(3), 160–175 (2019).
- Iafrazi, A., and Korobkin, A. A., "Initial stage of flat plate impact onto liquid free surface," *Phys. Fluids* **16**(7), 2214–2227 (2004).
- Iafrazi, A., and Korobkin, A. A., "Hydrodynamic loads during early stage of flat plate impact onto water surface," *Phys. Fluids* **20**(8), 082104 (2008).
- Ignatev, M., Kazarinov, N., and Petrov, Y., "Peridynamic modelling of the dynamic crack initiation," *Procedia Struct. Integrity* **28**, 1650–1654 (2020).
- IMO-2016. *The International Code for Ships Operating in Polar Waters* (International Maritime Organization, London, 2016).
- Jiao, J., and Ren, H., "Characteristics of bow-flare slamming and hydroelastic vibrations of a vessel in severe irregular waves investigated by segmented model experiments," *J. Vibroengineering* **18**(4), 2475–2494 (2016).
- Joukowski, N. E., "On impact of two spheres, one of which floats in liquid," *Zap. Mat. Otd. Novorossiiskogo Obschestva Estestvoispytatelej* **5**, 43–48 (1884).
- Kashiwagi, M., "Transient responses of a VLFS during landing and take-off of an airplane," *J. Mar. Sci. Technol.* **9**(1), 14–23 (2004).
- Kerr, A. D., "Elastic and viscoelastic foundation models," *J. Appl. Mech.* **31**(3), 491–498 (1964).
- Khabakhpasheva, T. I., Chen, Y., Korobkin, A. A., and Maki, K., "Water impact near the edge of a floating ice sheet," in Proceedings of 33rd International Workshop on Water Waves and Floating Bodies (2018a).
- Khabakhpasheva, T., Chen, Y., Korobkin, A. A., and Maki, K., "Impact onto an ice floe," *J. Adv. Res. Ocean Eng.* **4**(4), 146–162 (2018b).
- Khabakhpasheva, T., and Korobkin, A., "Elastic wedge impact onto a liquid surface: Wagner's solution and approximate models," *J. Fluids Struct.* **36**, 32–49 (2013).
- Kim, E., "Experimental and numerical studies related to the coupled behavior of ice mass and steel structures during accidental collisions," Doctoral thesis (NTNU Institutt for Marin Teknikk, Norway, 2014).
- Korobkin, A., "Unsteady hydroelasticity of floating plates," *J. Fluids Struct.* **14**(7), 971–991 (2000).
- Korobkin, A. A., "Wave impact on the center of an Euler beam," *J. Appl. Mech. Tech. Phys.* **39**(5), 770–781 (1998).
- Korobkin, A. A., and Khabakhpasheva, T. I., "Plane problem of asymmetrical wave impact on an elastic plate," *J. Appl. Mech. Tech. Phys.* **39**(5), 782–791 (1998).
- Korobkin, A. A., and Khabakhpasheva, T. I., "Regular wave impact onto an elastic plate," *J. Eng. Math.* **55**(1–4), 127–150 (2006).
- Korobkin, A. A., and Khabakhpasheva, T. I., "Impact on an ice floe with a surface crack," in *International Conference on Offshore Mechanics and Arctic Engineering* (American Society of Mechanical Engineers, 2018), Vol. 51302, p. V009T13A014.
- Korobkin, A. A., Khabakhpasheva, T. I., Ye, H., and Maki, K., "Vertical impact onto floating ice," in Proceedings of 25th International Symposium on Ice, Trondheim, Norway, 23rd–25th November 2020 (2020), pp. 473–482.
- Korobkin, A., and Malenica, S., "Rational assessment of fluid impact loads," in *UK Success Stories in Industrial Mathematics* (Springer, Cham, 2016), pp. 99–105.
- Korobkin, A. A., and Pukhnachov, V. V., "Initial stage of water impact," *Annu. Rev. Fluid Mech.* **20**(1), 159–185 (1988).
- Kozin, V. M., and Pogorelova, A. V., "Mathematical modeling of shock loading of a solid ice cover," *Int. J. Offshore Polar Eng.* **16**(01), ISOPE-06-16-1-001 (2006).
- Kvalsevold, J., "Slamming loads on wetdecks of multihull vessels," in *Proceedings of the International Conference on Hydroelasticity in Marine Technology, Trondheim, Norway, May 1994*, edited by O. Faltinsen *et al.* (Balkema, Rotterdam, The Netherlands, 1994), P1994–9, ISBN: 90 5410 387 6.
- Lau, M., Simões Ré, A., and Veitch, B., "Performance of survival craft in ice environments," in International Conference and Exhibition on Performance of Ships and Structures in Ice (2006), pp. 16–19.
- Loukakis, T. A., and Sfavounos, P. D., "Some extensions of the classical approach to strip theory of ship motions, including the calculation of mean added forces and moments," *J. Ship Res.* **22**(01), 1–19 (1978).
- Lubbard, R., and Loset, S., "A numerical model for real-time simulation of ship-ice interaction," *Cold Reg. Sci. Techn.* **65**(2), 111–127 (2011).
- Maki, K. J., Ye, H., Khabakhpasheva, T. I., and Korobkin, A. A., "Impact of a wedge-shaped body with influence of broken ice," in Proceedings of 32nd International Workshop on Water Waves and Floating Bodies (2017).
- Marchenko, A., Haase, A., Jensen, A., Lishman, B., Rabault, J., Evers, K. U., Shortt, M., and Thiel, T., "Laboratory investigations of the bending rheology of floating saline ice, and physical mechanisms of wave damping in the HSVA Hamburg Ship Model Basin Ice Tank," *Water* **13**(8), 1080 (2021).
- Morse, P. M., *Vibration and Sound* (McGraw-Hill Book Company, New York, 1948).
- Nakazawa, N., and Sodhi, D. S., *Ice Forces on Flat, Vertical Indentors Pushed Through Floating Ice Sheets* (Cold Regions Research and Engineering Laboratory, Hanover, NH, 1990).
- Peck, D. T., "Axisymmetric problems involving fractures with moving boundaries," Ph.D. thesis (Aberystwyth University, 2018).
- Petrov, Y. V., and Morozov, N. F., "On the modeling of fracture of brittle solids," *J. Appl. Mech.* **61**(3), 710–712 (1994).
- Petrovic, J. J., "Review mechanical properties of ice and snow," *J. Mater. Sci.* **38**(1), 1–6 (2003).
- Pogorelova, A. V., "Plane problem of the impact of several shock pulses on a viscoelastic plate floating on a fluid surface," *J. Appl. Mech. Tech. Phys.* **51**(2), 155–163 (2010).
- Qiu, L. C., "Numerical simulation of transient hydroelastic response of a floating beam induced by landing loads," *Appl. Ocean Res.* **29**(3), 91–98 (2007).
- Raykov, T., and Marcoulides, G. A., "On desirability of parsimony in structural equation model selection," *Struct. Eq. Model: A Multidiscip. J.* **6**(3), 292–300 (1999).
- Re, S., and Veitch, B., "Performance limits of evacuation systems in ice," in Proceedings of the 17th International Conference on Port and Ocean Engineering under Arctic Conditions, Trondheim, Norway, 2003, pp. 807–817.
- Schulson, E. M., "The structure and mechanical behavior of ice," *J. Met.* **51**(2), 21–27 (1999), available at <https://www.tms.org/pubs/journals/JOM/9902/Schulson-9902.html>.
- Sebastiro, P. J., "The art of model fitting to experimental results," *Euro. J. Phys.* **35**(1), 015017 (2013).
- Shams, A., Lopresto, V., and Porfiri, M., "Modeling fluid-structure interactions during impact loading of water-backed panels," *Compos. Struct.* **171**, 576–590 (2017).
- Shishmarev, K., Khabakhpasheva, T., and Korobkin, A., "Ice response to an underwater body moving in a frozen channel," *Appl. Ocean Res.* **91**, 101877 (2019).
- Sodhi, D. S., "Interaction forces during vertical penetration of floating ice sheets with cylindrical indentors," in Proceedings of 8th International Conference on Offshore Mechanics and Arctic Engineering (1989), Vol. IV, p. 377.
- Sodhi, D. S., "Vertical penetration of floating ice sheets," *Int. J. Solids Struct.* **35**(31–32), 4275–4294 (1998).
- Squire, V., Hosking, R. J., Kerr, A. D., and Langhorne, P., *Moving Loads on Ice Plates* (Springer Science & Business Media, 1996), p. 45.
- Sun, H., and Faltinsen, O. M., "Dynamic motions of planing vessels in head seas," *J. Mar. Sci. Technol.* **16**(2), 168–180 (2011).

- Tassin, A., Piro, D. J., Korobkin, A. A., Maki, K. J., and Cooker, M. J., "Two-dimensional water entry and exit of a body whose shape varies in time," *J. Fluids Struct.* **40**, 317–336 (2013).
- Tkacheva, L. A., "Motion of a system of seismic sources over ice on a body of water under the action of a pulse," *J. Appl. Mech. Tech. Phys.* **48**(2), 271–278 (2007).
- Watanabe, E., Utsunomiya, T., and Tanigaki, S., "A transient response analysis of a very large floating structure by finite element method," *J. Struct. Mech. Earthquake Eng.* **598**, 1–9 (1998), available at https://www.jstage.jst.go.jp/article/jscej1984/1998/598/1998_598_1/_pdf.
- Ye, L. Y., Guo, C. Y., Wang, C., Wang, C. H., and Chang, X., "Peridynamic solution for submarine surfacing through ice," *Ships Offshore Struct.* **15**(5), 535–549 (2020).
- Younesian, D., Hosseinkhani, A., Askari, H., and Esmailzadeh, E., "Elastic and viscoelastic foundations: A review on linear and nonlinear vibration modeling and applications," *Nonlinear Dyn.* **97**, 853–895 (2019).
- Zakki, A. F., Windyandari, A., and Bae, D. M., "The development of new type free-fall lifeboat using fluid structure interaction analysis," *J. Mar. Sci. Technol.* **24**(3), 575–580 (2016).